Molecular Dynamics Study of Sodium Octanoate Self-assembly in Parallel-Wall Confinements

by

Mohammod Hafizur Rahman

Submitted in partial fulfilment of the requirements
for the degree of Doctor of Philosophy

at

Dalhousie University
Halifax, Nova Scotia
April 2012

DALHOUSIE UNIVERSITY

PROCESS ENGINEERING AND APPLIED SCIENCE

The undersigned hereby certify that they have read and recommend to the Faculty of Graduate Studies for acceptance a thesis entitled "Molecular Dynamics Study of Sodium Octanoate Self-assembly in Parallel-Wall Confinements" by Mohammod Hafizur Rahman in partial fulfilment of the requirements for the degree of Doctor of Philosophy.

Dated: April 23, 2012

External Examiner: _____

Research Co-Supervisors: _____

_____

Examining Committee: _____

_____

_____

Departmental Representative: _____

DALHOUSIE UNIVERSITY

DATE: April 23, 2012

AUTHOR: Mohammod Hafizur Rahman

TITLE: Molecular Dynamics Study of Sodium Octanoate Self-assembly in Parallel-Wall Confinements

DEPARTMENT OR SCHOOL: Process Engineering and Applied Science

DEGREE: PhD CONVOCATION: October YEAR: 2012

_____

Signature of Author

Table of Contents

List of Tables vii

List of Figures viii

Abstract xv

List of Abbreviations and Symbols Used xvi

CHAPTER 1: INTRODUCTION 1

1.1 Confined Fluids 3

1.2 Surfactant Micellization 4

1.3 Shape of Surfactant Aggregates 5

1.4 Molecular-Thermodynamic Framework of Micellization 6

1.5 Surfactant Adsorption on Solid Surfaces 8

1.6 Molecular Dynamics Simulation of Surfactant 10

1.7 Objectives 12

CHAPTER2: METHODOLOGY 14

2.1 Simulation Model 14

2.2 Simulation Procedure 16

2.3 Potential of Mean Force 18

2.4 Aggregate Size Determination 19

2.5 Surfactant Adsorption 20

2.6 Density Distribution 21

2.7 Radial Distribution Function 22

2.8 Water Structure 22

CHAPTER 3: SIMULATION OF BULK SODIUM OCTANOATE SOLUTIONS AND CHARACTERIZATION OF THE WALLS 24
3.1 Introduction 24
3.2 Micelle Formation in Sodium Octanoate Solutions 25
3.3 Critical Micelle Concentration 27
3.4 Characterization of Confining Walls 28
3.5 Concluding Remarks 30
CHAPTER 4: SODIUM OCTANOATE CONFINED BY TWO PARALLEL GRAPHITE WALLS 31
4.1 Introduction 31
4.2 Micelle Formation in Confinement 31
4.3 Effect of Surfactant Concentration on Adsorption 34
4.4 Effect of Concentration on Micelle Size 37
4.5 Effect of Gap Size on Adsorption 42
4.6 Effect of Gap Size on Micelle Formation 43
4.7 Water Structure in Confined SO Solutions 46
4.8 Concluding Remarks 48
CHAPTER 5: SODIUM OCTANOATE CONFINED BETWEEN TWO PARALLEL HYDROPHILIC AND HYDROPHOBIC SILICA WALLS 50
5.1 Introduction 50
5.2 Bilayer Formation between Two Hydrophilic Silica Walls 50
5.3 Effect of Surfactant Concentration and Gap Size in Hydrophilic Silica Cases 57
5.4 Bilayer Formation between Two Hydrophobic Silica Walls 62
5.5 Hydrophobic and Electrostatic Interactions in Silica Confinement 67
5.6 Water Orientation and Bridge Structure 70
5.7 Concluding Remarks 71

CHAPTER 6: CONCLUSION AND FUTURE WORK 72
6.1 Future Work 73
References 76

List of Tables

Table 2.1: Charges on surface Si-O-H groups (hydrophilic plates)……..17

Table 4.1: Gap sizes and concentration ranges for the simulation studies of sodium octanoate solutions confined between two parallel graphite walls. 32

Table 4.2: Surfactant adsorption and aggregate size variation in sodium octanoate (SO) solutions confined between two parallel graphite walls with a gap size of 4 nm. 37

Table 4.3: Adsorption of octanoate molecules in sodium octanoate (SO) solutions confined between two parallel graphite walls. 40

Table 5.1: Simulation cases considered in the study of hydrophilic silica confinement..... 51

Table 5.2: Simulation cases considered in the study of hydrophobic silica confinement..... 63

List of Figures

Figure 1.1: Two types of surfactant aggregates: (a) spherical micelle and (b) planar bilayer. The yellow circles represent the hydrophilic "heads" of a surfactant molecule, and the black lines represent the hydrophobic "tails" of the molecule. 2

Figure 2.1: Molecular structure of sodium octanoate. 15

Figure 2.2: A snapshot depicting a sodium octanoate solution confined between two graphite walls……15

Figure 2.3: Snapshots of the hydrophilic silica wall showing (a) view of the *x*–*y* plane and (b) view of the *y*–*z* plane. (c) A SiO_4H unit. Red, yellow, and white spheres represent oxygen, silicon, and hydrogen atom, respectively. 16

Figure 2.4: Potential of mean force of a methane–methane pair in ambient water (SPC). 20

Figure 2.5: Potential of mean force between a methane molecule and the graphite wall. A methane molecule is confined by two parallel graphite walls with a gap size of 4 nm. The methane molecule is pulled from the center of mass of the confined water molecules. 21

Figure 2.6: Schematic diagram depicting the angle θ_{OH} formed between the O–H bond of a water molecule and the inward normal to the wall. 23

Figure 3.1: Simulated time variation of maximum aggregation number, n_m, in a 0.55 M sodium octanoate solution. 25

Figure 3.2: Average number densities of water (H_2O), counterion (Na^+), and various atomic groups of the octanoate molecule in a 0.55 M sodium octanoate solution. The distance *r* is measured from the center of mass of the aggregate. The average is taken from 60 ns to 80 ns. C denotes the methylene groups of the octanoate tail, C1 denotes the carbon atom attached to the oxygen atoms, and O denotes the oxygen atoms of octanoate. 26

Figure 3.3: Simulated time variation of maximum aggregation number, n_m, in bulk sodium octanoate solutions at various concentrations between 0.37 M and 0.55 M. 27

Figure 3.4: Density profiles of water along the *z*-axis. Pure water is confined by two parallel walls (siH: hydrophilic silica, si: hydrophobic silica, gr: graphite) with a gap size of 4 nm. Here *z* represents the distance from the inner surface of the wall. For the hydrophobic silica wall, the inner surface is located at the plane of the surface O atoms, whereas for the hydrophilic silica wall, the plane of the surface H atoms is considered as the inner surface. 28

Figure 3.5: Probability distribution, $P(\theta_{OH})$, of angle θ_{OH} between hydrogen bond vectors of water molecules and the normal direction to the plates, for molecules at a distance $\leq$0.1 nm in case of hydrophilic and hydrophobic silica wall and $\leq$0.30 for graphite wall. Water is confined by two parallel walls with a gap size of 4 nm. Legends represent the types of wall. 29

Figure 4.1: Density profiles of water (H_2O), counterion (Na^+), and various atomic groups of the octanoate molecule along the *z*-axis. A 2.1 M sodium octanoate solution is confined between two parallel graphite walls with a gap size of 4 nm. O, C1, and C8 denotes the oxygen atoms, the first carbon atom (attached to the oxygen atoms), and the last carbon atom of the octanoate molecule, respectively. 32

Figure 4.2: Snapshot of a 2.1 M sodium octanoate solution confined between two graphite walls, located above and below the solution layer, with a gap size of 4 nm (after 80 ns of simulation). The gray, red, and blue spheres represent carbon, oxygen, and Na^+, respectively. Water molecules and the two graphite walls have been removed for clarity. 33

Figure 4.3: Average number density distributions from the center of mass ($r = 0$) of the largest aggregate formed between two parallel graphite walls (gap size = 4 nm). The concentration of the confined sodium octanoate solution is 2.1 M. (a) C and H_2O denote the carbon atoms of the octanoate molecule and water, respectively. (b) C1 and O denote the first carbon atom (attached to the oxygen atoms) and the oxygen atoms of the octanoate molecule, respectively. Na^+ represents the counterion. 35

Figure 4.4: Density profiles of the C8 atom (end of surfactant tail) of the octanoate molecule for different surfactant concentrations. The SO solutions are confined between two parallel graphite walls with a gap size of 4 nm. 36

Figure 4.5: Potential of mean force between an octanoate anion and graphite wall. An octanoate anion and a Na^+ counterion are confined by two parallel graphite walls with a gap size of 4 nm. The octanoate anion is pulled from the center of mass of the confined water molecules. 36

Figure 4.6: Average number density distributions from the center of mass ($r = 0$) of the largest aggregate formed between two walls with a gap size of 4 nm. The concentrations of the confined sodium octanoate solution are (a) 1.9 M and (b) 2.3 M. C and H_2O denote the carbon atoms of the octanoate molecule and water, respectively. C1 and O denote the first carbon atom (attached to the oxygen atoms) and the oxygen atoms of the octanoate molecule, respectively. Na^+ represents the counterion. 38

Figure 4.7: Average number density distributions of the oxygen atoms from the center of mass ($r = 0$) of the largest aggregate formed between two walls with a gap size of 4 nm. The labels are the surfactant concentrations of the confined sodium octanoate solutions. 39

Figure 4.8: Variation of the ratio of moment of inertia, $<Ixx/Iyy>/<Izz/Iyy>$, of the aggregate as a function of surfactant concentration, where I_{kk} denotes the moment of inertia around the k-axis through the center of mass of the aggregate. The labels are the gap sizes. 40

Figure 4.9: Variation of aggregation number with surfactant concentration for aggregates formed between two parallel graphite walls with a gap size of 4 nm ("confined") and in a bulk solution ("bulk"). The data for the bulk solution were taken from the experimental study by Zemb *et al*. (1983). 41

Figure 4.10: Density profiles of the last carbon atom (C8) and the oxygen atoms (O) of the octanoate molecule in a sodium octanoate (SO) solution confined by two parallel graphite walls with gap sizes of 3 nm and 4 nm. The SO solution contains 72 SO molecules. z^* is the distance from the mid-plane scaled by half of the gap size. 43

Figure 4.11: Potential of mean force between two methane molecules. The case in which two methane molecules are confined between two parallel graphite walls with a gap size of 4 nm is labeled as "confined", and the corresponding case in bulk water in labeled as "bulk". 45

Figure 4.12: Potential of mean force between two CH_3COO^- ions. The case in which two sodium octanoate are confined between two parallel graphite walls with a gap size of 4 nm is labeled as "confined", and the corresponding case in bulk water in labeled as "bulk". 45

Figure 4.13: Density profiles of the oxygen atoms (O) and the C8 atom of the octanoate molecule in a 2.0 M sodium octanoate solution confined by two parallel graphite walls with a gap size of 3 nm. The distance z is the distance from the mid-plane along the z direction. 47

Figure 4.14: Probability distributions, $P(\theta_{OH})$, of the angle θ_{OH} between the water O–H bond and the inward normal to the wall. The water molecules are contained in different water layers, each 0.1 nm thick, at three locations (z = 0, 0.5, and 1.0 nm from the mid-plane). A 2.0 M sodium octanoate solution is confined by two parallel graphite walls with a gap size of 3 nm. 47

Figure 4.15: Probability distributions, $P(\theta_{OH})$, of the angle θ_{OH} between the water O–H bond and the inward normal to the wall. The water molecules are contained in different water layers, each 0.1 nm thick, at four locations (z = 0, 0.5, 1.0, and 1.5 nm from the mid-plane). Pure water is confined by two parallel graphite walls with a gap size of 4 nm. 48

Figure 5.1: Time-averaged density distributions of various atomic groups along the z-axis in a 2.09 M sodium octanoate solution confined by two hydrophilic silica walls with a gap size of 4 nm. The distance z is the distance from the mid-plane of the two walls. The average was taken from the frames between 80 ns and 120 ns. C and O denote the methylene groups and the oxygen atoms of octanoate, respectively. Na^+ and H_2O carry their usual meaning. 52

Figure 5.2: Snapshot (interfacial region) of sodium octanoate solution confined by two hydrophilic (hydroxylated) silica walls with a gap size of 4 nm and a concentration of 2.09 M (at 80 ns). Gray spheres represent the methylene groups of the octanoate molecule, red spheres represent oxygen atoms, blue spheres are Na^+ ion, yellow spheres represents silicon atoms, and white spheres represents hydrogen atoms. Water molecules are represented by green spheres. 53

Figure 5.3: Time-averaged density distributions of the C1 and C8 atoms of the octanoate molecule along the z-axis in a 2.1 M sodium octanoate solution confined by two hydrophilic silica walls (gap size = 4 nm). The average was taken from the frames between 80 ns and 120 ns. C1 and C8 denote the first carbon atom and terminal methyl group, respectively, of the octanoate molecule from the head end. The distance z represents the distance from the mid-plane of the two walls. 53

Figure 5.4: Snapshots of a sodium octanoate solution confined by two hydrophilic silica (hydroxylated) walls with a gap size of 4 nm at a surfactant concentration of 2.09 M (at 80 ns). (a) y–z plane and (b) x–z plane. Gray spheres represent the methylene groups of an octanoate molecule, red spheres represent oxygen atoms, blue spheres are Na^+ ion, yellow spheres represent silicon atoms, and white spheres represent hydrogen atoms. Water molecules have been removed for clarity. 54

Figure 5.5: Potential of mean force between a methane (CH_4) molecule and the hydrophilic silica wall ("siH"), and between a CH_4 molecule and the hydrophobic silica wall ("si"). A CH_4 molecule is confined between two parallel silica walls with a gap size of 4 nm. 55

Figure 5.6: Potential of mean force between an acetate (CH_3COO^-) ion and a hydrophilic silica wall ("siH"), and between a CH_3COO^- ion and a hydrophobic silica wall ("si"). A CH_3COO^- ion and a Na+ ion are confined between two parallel silica walls with a gap size of 4 nm. 55

Figure 5.7: Radial distribution functions (RDFs) between a Na^+ ion and the oxygen atoms of an octanoate molecule in a 0.55 M sodium octanoate (SO) solution ("bulk") and in a 2.1 M SO solution confined by two parallel hydrophilic silica walls with a gap size of 4 nm ("siH"). The RDFs were calculated from the frames between 80 ns and 120 ns. 56

Figure 5.8: Radial distribution functions (RDFs) between two C1 atoms of the octanoate molecule in a 0.55 M sodium octanoate (SO) solution ("bulk") and in a 2.1 M SO solution confined by two parallel hydrophilic silica walls with a gap size of 4 nm ("siH"). The RDFs were calculated from the frames between 80 ns and 120 ns. 57

Figure 5.9: Radial distribution functions (RDFs) between a Na^+ ion and the oxygen atoms of an octanoate molecule at different concentrations. The sodium octanoate solution is confined between two parallel hydrophilic silica walls with a gap size of 4 nm. The RDFs were calculated from the frames between 80 ns and 120 ns. 58

Figure 5.10: Time-averaged density distributions of the (a) C8 and (b) C1 atoms of octanoate along the *z*-axis in a sodium octanoate solution confined by two parallel hydrophilic silica walls with a gap size of 4 nm at different concentrations. C1 is attached to the two oxygen atoms and C8 is located at the tail end. The distance *z* represents the distance from the mid-plane of the two walls. The average is taken from the frames between 80 ns and 120 ns. 59

Figure 5.11: Time-averaged density distribution of the C8 and C1 atoms of octanoate along *z*-axis in a sodium octanoate solution confined by two parallel hydrophilic silica walls with a gap size of 5 nm and a surfactant concentration of 1.47 M. C1 is attached to the two oxygen atoms and C8 is located at the tail end. The distance *r* represents the distance from the mid-plane of the two walls. The average is taken from the frames between 80 ns and 120 ns. 60

Figure 5.12: Snapshots of sodium octanoate solutions confined between two hydrophilic silica (hydroxylated) walls with a gap size of 5 nm at different concentrations (at 80 ns). (a) 1.47 M, (b) 1.54 M, (c) 1.68 M. Gray spheres represent the methylene groups of the octanoate molecule, red spheres represent oxygen atoms, blue spheres are Na^+ ion, and yellow spheres represents silicon atoms. Water molecules have been removed for clarity. 61

Figure 5.13: Snapshots of sodium octanoate solutions confined by two hydrophilic silica (hydroxylated) walls with a gap size of 6 nm at different concentration (at 80 ns). (a) 1.25 M, (b) 1.50 M. Gray spheres represent the methylene groups of the octanoate molecule, red spheres represent oxygen atoms, blue spheres are Na^+ ion, and yellow spheres represents silicon atoms. Water molecules have been removed for clarity. 62

Figure 5.14: Time-averaged density distributions of various atomic groups along the *z*-axis in a 2.1 M sodium octanoate solution confined by two hydrophobic silica walls with a gap size of 4 nm. The distance *z* is the distance from the mid-plane of the two walls. The average was taken from the frames between 80 ns and 120 ns. C and O denote the methylene groups and the oxygen atoms of octanoate. respectively. Na^+ and H_2O carry their usual meaning. 64

Figure 5.15: Partial snapshot showing the solid–liquid interface in a 2.1 M sodium octanoate solution confined by two hydrophobic silica walls with a gap size of 4 nm (at 80 ns). Gray spheres represent the methylene groups of the octanoate molecule, red spheres represent oxygen atoms, blue spheres are Na^+ ion, and yellow spheres represents silicon atoms. Water molecules are represented by green spheres. 64

Figure 5.16: Time-averaged density distributions of the C1, C8, and oxygen atoms (O) of octanoate along the *z*-axis in a 2.1 M sodium octanoate solution confined by two hydrophobic silica walls with a gap size of 4 nm. The distance *z* is the distance from the mid-plane of the two walls. The average was taken from the frames between 80 ns and 120 ns. C1 and C8 represent the first carbon atom and the terminal methyl group, respectively, of octanoate from the head end. 65

Figure 5.17: Snapshots of a 2.1 M sodium octanoate solution confined by two hydrophobic silica walls with a gap size of 4 nm (at 80 ns). (a) *y*–*z* plane and (b) *x*–*z* plane. Gray spheres represent the methylene groups of an octanoate molecule, red spheres represent oxygen atoms, blue spheres are Na^+ ion, and yellow spheres represent silicon atoms. Water molecules have been removed for clarity. 66

Figure 5.18: Snapshot of a 1.75 M sodium octanoate solution confined between two hydrophobic silica walls with a gap size of 6 nm (at 80 ns). (a) *y*–*z* plane and (b) *x*–*z* plane.Gray spheres represent the methylene groups of an octanoate molecule, red spheres represent oxygen atoms, blue spheres are Na^+ ion, and yellow spheres represent silicon atoms. Water molecules have been removed for clarity. 67

Figure 5.19: Potential of mean force between two methane molecules in water at infinite dilution ("bulk") and confined between two hydrophilic silica walls ("siH") and two hydrophobic silica walls ("si") with a gap size of 4 nm. 68

Figure 5.20: Potential of mean force between CH_3COO^- and Na^+ in water at in finite dilution ("bulk") and confined between two hydrophilic silica walls ("siH") and two hydrophobic silica walls ("si") with a gap size of 4 nm. 69

Figure 5.21: Potential of mean force between two CH_3COO^- ions in water at in finite dilution ("bulk") and confined between two hydrophilic silica walls ("siH") and two hydrophobic silica walls ("si") with a gap size of 4 nm……..70

Abstract

The practical applications of surfactant solutions in confined geometries require a thorough understanding of the system properties. Coarse-grained simulation techniques are useful for studying the qualitative behaviour of these systems, whereas the atomistic molecular dynamics (MD) technique can be used to obtain a molecular-level description. In this work, canonical MD simulations were performed using GROMACS version 4.0 to investigate the self-assembling behaviour of sodium octanoate (SO) confined between two parallel walls. In particular, the effects of gap size, wall type, and surfactant concentrations on the morphology of the surfactant aggregates were studied to gain in-depth knowledge of the system.

The simulation results reveal that the morphology of the micelles formed between two parallel walls are affected not only by the gap size and surfactant concentration, but also by the nature and characteristics of the confining walls. With the graphite walls, most octanoate molecules are adsorbed at lower concentrations, but they form micellar aggregates as the surfactant concentration increases. Spherical micelles were found in the larger gaps (4 nm and 5 nm) but not in the smaller gap (3 nm), and the micellar shape also changes with increasing surfactant concentration. SO forms bilayer structures instead of spherical micelles between two silica walls. Interestingly, in the hydrophilic silica confinement, the orientation of these bilayers changes with gap sizes, whereas in the hydrophobic silica confinement, these bilayers remain perpendicular to the wall in all cases.

Potentials of mean force between different molecules and atomic groups were determined under different conditions in order to develop a better understanding of the simulation results. It reveals, the presence of the confinement can alter the intermolecular interactions among the surfactant molecules, which, in turn, directly affects the self-assembling process, particularly the size and shape of the aggregates. Indeed, the formation of bilayers in silica wall confinement, as opposed to spherical micelles in graphite confinement, is caused by the enhanced electrostatic interactions between the charged atoms in the solution. The results of this study are expected to provide further insight into the self-assembling behaviour of confined surfactant systems, and may ultimately lead to the development of novel nanomaterials.

List of Abbreviations and Symbols Used

COM	Center of Mass
CMC	Critical Micelle Concentration
GROMACS	Groningen Machine For Chemical Simulations
GROMOS	Groningen Molecular Simulation Package
LINCS	Linear Constraint Solver
MD	Molecular Dynamics
PME	Particle-Mesh Ewald
PMF	Potential of Mean Force
RDF	Radial distribution function
SDS	Sodium Dodecyl Sulfate
SO	Sodium Octanoate
SPC	Simple Point Charge
n_m	Maximum aggregation number

CHAPTER 1

INTRODUCTION

Surfactants are used extensively in many consumer and industrial products, including detergents, coatings, and dispersions. They are also used in various chemical and medical applications, such as catalysis, electronics manufacturing, lubrication, mineral flotation, and drug delivery. Because a surfactant molecule contains both hydrophobic and hydrophilic parts, aqueous surfactant solutions possess unique solution and interfacial characteristics (Verwey and Ovrbeek, 1948). In addition to their ability to reduce surface and interfacial tensions, surfactants can self-assemble in aqueous solutions to form a variety of aggregates such as micelles, vesicles, and lamellae (see Figure 1.1).

Most surfactant formulations, such as detergents and coatings, are applied in the form of bulk solutions. However, in some specialized operations, surfactants are used in small confined space. For example, in the surfactant-facilitated groundwater remediation, surfactants are used to enhance solubilization of trapped organic materials in porous soils (West and Harwell, 1992). In the petroleum industry, surfactant solutions are injected into porous media in a number of applications (Schramm *et al.*, 1994). It is therefore important to develop a detailed understanding of the behaviour of these complex fluids, including their equilibrium structure and transport properties, under confinement (Sahimi, 1993). This enhanced knowledge will not only facilitate existing applications of surfactant solutions in porous media, but also help to exploit the unique properties of confined surfactant solutions in developing new technologies. For example, in oil and gas drilling, one of the challenges is to formulate a drilling fluid that can minimize wellbore instability and drilling costs while meeting stringent environmental regulations. Water-based drilling fluids, while being environmentally friendly, often interact with shale and cause serious drilling problems such as hole enlargement and pack-off. Since shale is essentially a medium composed of very small charged pores,

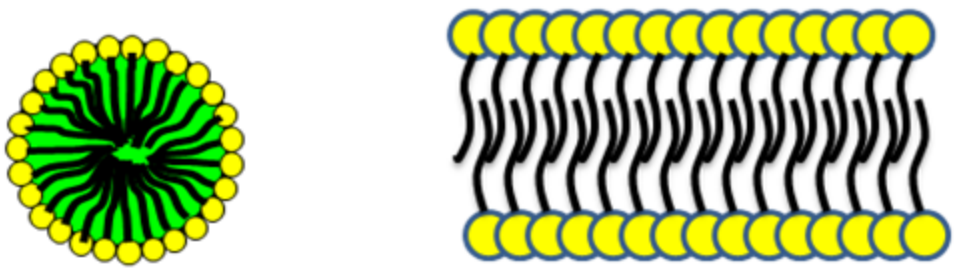

(a) (b)

Figure 1.1: Two types of surfactant aggregates: (a) spherical micelle and (b) planar bilayer. The yellow circles represent the hydrophilic "heads" of a surfactant molecule, and the black lines represent the hydrophobic "tails" of the molecule.

with diameters ranging from a few to tens of nanometers (Katsube *et al.*, 1991), it is conceivable that microphase separation in a surfactant solution within a shale pore may help to reduce water influx. One possible mechanism involves the transition of small spherical micelles to elongated, worm-like micelles, which behave more like polymers, hence inducing changes in local viscosity. In groundwater cleanup, it has also been shown that flow of latex microspheres can facilitate contaminant transport in porous media (Roy and Dzombak, 1997). Thus, self-assembling colloids formed with biodegradable surfactants, such as the relatively new class of polyhydroxyl-based surfactants, may offer more flexibility in terms of size and solubilization capacity, in addition to the environmental advantage (Soderman and Johansson, 1999). In the development of novel nanomaterials, the ability of amphiphilic compounds to self-assemble into well-defined structures is used for the synthesis of inorganic materials with nanometer dimensions (Holmberg *et al.*, 2004; Anilkumar and Jayakannan, 2007; Vasudevan *et al.*, 2010). Thus, if the shape of a micelle can be manipulated using external forces, such a technique may expand the capability of nanomaterial manufacturing.

1.1 Confined Fluids

The structural properties of simple fluids confined in narrow slits or pores have been the subject of theoretical interest for many years because of their relevance to practical application as well as their association with interesting phenomena such as selective adsorption from mixtures, solvation forces in liquids, etc. (Henderson,1992; Cracknell *et al.*, 1995). The driving force in all these cases is the wall–fluid interaction, which leads to an inhomogeneous density distribution of the components inside the confined space, especially near the wall. The behaviour of a thin water film confined by hydrophilic and hydrophobic walls has also attracted considerable attention. Ju *et al.* (2005) showed that the structure of water confined by two Au(001) walls was affected by the width of the gap, and they found that the distribution of the water molecules changed as the gap widened. In a study of water molecules at an uncharged graphite wall interface, Hirunsit and Balbuena (2007) observed that the mobility of the water molecules was reduced at the vicinity of the wall. A water film can also be thermodynamically destabilized when it is confined between two hydrophobic surfaces approaching each other at a small separation distance (Leung *et al.*, 2003; Choudhury and Pettitt, 2005).

Unlike simple fluids, the behaviour of confined surfactant solutions has received relatively little attention (Gersappe, 2000). Intuitively, the effects of confinement would depend on the relative length scale. If the pore is much larger than the surfactant aggregate, the surfactant solution is expected to behave as a bulk solution. On the other hand, if the pore size is comparable to the aggregate size, or if the pore wall is charged, the thermodynamic and rheological behaviour of the solution may be very different (Lee, 2008). Indeed, it has been observed that long-range attractive interactions may exist between like-charged colloids near a charged surface, and block copolymer micelles adopt an ordered structure in two-dimensional confinement (Ise *et al.*, 1983; Kepler and Fraden, 1994; Esselink *et al.*, 1995; Crocker and Grier, 1996a; Crocker and Grier, 1996b; Carbajal-Tinoco *et al.*, 1996; Grier, 1997; Larsen and Grier, 1997).

1.2 Surfactant Micellization

In an aqueous surfactant solution, micellization occurs when the surfactant concentration reaches a level known as the critical micelle concentration (CMC). Below the CMC, the hydrophobicity of a surfactant tail causes the structuring of the water molecules surrounding the tail, resulting in a decrease of the system entropy. At the CMC, the interactions among the surfactant tails become stronger, and the surfactant molecules begin to aggregate, thus releasing the structured water surrounding the tails. This effect is known as the "hydrophobic effect," which is the major driving force for micellization (Tanford, 1980). As the surfactant molecules assemble into aggregates, the hydrophilic head groups also form a "shield" to minimize water–hydrocarbon contacts.

Kinetic studies of micellar solutions have shown that individual amphiphiles are free to leave a micelle and diffuse within the solution as monomers, before joining other micelles (Mittal, 1977). In other words, micellar aggregates are chemical species which reversibly exchange portions of themselves with one another. As a result, individual micelles do not have a distinct identity; they have no definite size, only a size distribution around some mean values. A description of the state of a micellar solution consists of a statistical specification of the distribution of micellar sizes which exists on average in the solution.

Surfactant molecules in a micelle are held together by van der Waals forces, hydrophobic forces, hydrogen bonds, and screened electrostatic interactions. These are weak forces compared to the strong covalent or ionic bond; thus, solution conditions such as temperature, electrolyte concentration, and pH would affect the intermolecular forces within each aggregate, as well as the interactions between aggregates, thereby modify the size and shape of the structures (Israelachvili, 1992).

Eriksson *et al.* (1981) described the thermodynamics of micelle formation, and explained that the free energy change associated with micelle formation consists of two parts: (i) a negative contribution (lowering of free energy) because of the replacement of the hydrocarbon–water contacts with hydrocarbon–hydrocarbon contacts, and (ii) a positive contribution (increase of free energy) originating from the repulsive interactions between the polar head groups at the surface of the micelle. Inside the micelle, the

surfactant tails interact through attractive hydrophobic forces, whereas the polar head groups tend to repel each other. The balance between these repulsive and attractive forces results in different micelle structures. When a surfactant solution is confined within a small space, however, the confinement itself would induce an external force to the system (Lee, 2008). The application of any external forces would, in principle, distort the balance among the forces responsible for micellization and produce different characteristics in a surfactant solution by altering its equilibrium state.

1.3 Shape of Surfactant Aggregates

The shape of a micelle affects various properties of a surfactant solution, including its viscosity. Most micelles are spherical and are relatively small, with an aggregation number of 100 or smaller. However, aggregates of other shapes, such as elongated cylinder, planar lamella, and vesicle, may form under different solution conditions. Israelachvili *et al.* (1976, 1977) developed a theory to describe micellar structure. The theory is based on the geometry of the surfactant molecule, particularly the space occupied by the hydrophilic and the hydrophobic groups. A packing parameter, calculated as $V_H/l_c a_o$, was introduced. Here, V_H is the volume occupied by the tail in the micellar core, l_c is the tail length, and a_o is the area occupied by the hydrophilic head group at the micelle–solution interface. As the value of this packing parameter changes from zero to one, the shape of the micelle also changes from spheroidal to lamellar. The value of a_o depends on the structure of the hydrophilic head group, which also varies with electrolyte content, pH, and the presence of additives in the solution. In solutions containing ionic surfactants, as the electrolyte concentration increases, the compression of the electric double layer reduces the magnitude of a_o. In case of confined surfactant solutions, it is conceivable that external forces also affect the packing parameter, causing the surfactant aggregates to adopt a shape different from that in bulk solutions. This point will be discussed in more detail in the following section.

1.4 Molecular-Thermodynamic Framework of Micellization

Molecular-thermodynamic theory provides a detailed account of the micellization process in a bulk surfactant solution (Hines, 2001). A number of researchers have worked to develop an accurate theoretical model of surfactant micellization (Blankschtein *et al.*, 1986; Nagarajan and Ruckenstein, 1991; Puvvada and Blankschtein, 1990). Blankschtein and co-workers (1986, 1990, 1992a, 1992b) presented a phenomenological theory, which has been widely cited in the literature (Yuet and Blankschtein, 1996; Shiloach and Blankschtein, 1998; Sohrabi *et al.*, 2007; Rodriguez-Pulido *et al.*, 2010; Sohrabi *et al.*, 2010). This theory constitutes an effort to include in a single, unified theoretical framework the effects of both intermicellar interactions and multiple chemical equilibria on the micellar size distribution and the equilibrium thermodynamic properties in both the single-phase and the two-phase regions of micellar solutions. They developed an expression for the free energy, which describes the essential equilibrium physical features of the thermodynamics of micellar solutions. These features include: (i) the free energy change associated with the formation of micelles, G_{f}, (ii) the free energy of mixing, G_{m}, which describes the number of geometric configurations available to all the species in solution, and (iii) the interaction free energy, G_{i}, between the micelles. The total system free energy is then expressed as

$$G = G_{\mathrm{f}} + G_{\mathrm{m}} + G_{\mathrm{i}} \tag{1.1}$$

In a confined surfactant solution, the number of configurations available to the molecules may be different from that in a bulk solution, which may affect the free energy of mixing, G_{m}. The interaction free energy, G_{i}, reflects the interactions between the micellar aggregates, the monomeric amphiphiles, and the water molecules. Blankschtein *et al*. (1986) adopted a mean-field form for this free energy as given by

$$G_{\mathrm{i}} = -(1/2)\sum_i N_i\, U_i \tag{1.2}$$

where $U_i = U\ \sum_j f_{ij}\rho_j$, f_{ij} is a coupling constant describing how the average interaction between an *i*-mer and a *j*-mer depends on the number of amphiphiles *i* and *j* in each of them, $\rho_j = N_j/\Omega$ is the number density of the *j*-mer, N_j is the number of *j*-mer, and Ω is the average volume of the solution. This expression for G_{i} assumes that each *i*-mer is

interacting with an average local potential U_i produced by other j-mers, and the parameter $U(T, P)$ measures the magnitude of the potential. In contrast, in the case of confined micellar solutions, the interactions between the confining walls and the various species in solution should also be counted. As the confinement becomes smaller, the wall–surfactant interactions will become more important, and it is reasonable to expect that, in very small confinements, the interactions between the walls and the micellar aggregates will be comparable to the intermicellar interactions. In addition, the presence of the confining walls would break the spherical symmetry found in a bulk solution, which may restrict the validity of the mean-field approximation used in eq 1.2.

As noted in many previous studies, the interactions among colloidal particles and micellar aggregates in confined geometries can be very different from those in bulk solutions (Choudhury and Ghosh, 1999; Mileva, 2000; Goulding and Hansen, 1998; Crocker and Grier, 1996a; Kepler and Fraden 1994; Crocker and Grier, 1996b; Grier, 1997; Ise *et al.*, 1983; Carbajal-Tinoco *et al.*, 1996). Experimental observations suggest that strong long-range attractions may exist between colloidal spheres confined to a plane by charged glass walls (Crocker and Grier, 1996a; Kepler and Fraden, 1994), and such attractions vanish as the confining walls are drawn apart (Crocker and Grier, 1996b). Bowen and Sharif (1998) showed that this type of interparticle attraction may be explained by the redistribution of the electric double layers of ions and counterions in the solution around the spheres caused by the presence of the walls. Thus, in a confined surfactant solution, it is expected that the confinement would distort the intermicellar interactions and lead to a different micellar behaviour compared to a bulk solution.

The free energy of formation for a bulk surfactant solution containing N_w water molecules and N_s surfactant molecules can be expressed as

$$G_f = N_w\mu_w^0 + N_s\mu_s^0 + \sum_n\{nN_n g_{mic}(n, l_c, Sh)\} \qquad (1.3)$$

where $\mu_w^0(T, P)$ and $\mu_s^0(T, P)$ are the standard-state chemical potentials of water and surfactant monomers, respectively, at the solution temperature T and pressure P, N_n is the number of aggregates with an aggregation number n, and $g_{mic}(n, l_c, Sh)$ is the free energy of micellization, which represents the free energy change per molecule associated

with forming a micelle of aggregation number n, core minor radius l_c, and shape Sh (sphere, cylinder, etc.). The standard state is taken as the surfactant monomer in aqueous solution. The free energy of micellization reflects the tendency of micelle formation and growth. It describes many complex physicochemical factors responsible for micelle formation, including the hydrophobic effect, hydrogen bonding, conformational changes associated with the packing of hydrophobic tails in the micellar core, and steric and electrostatic interactions between the hydrophilic head groups (Srinivasan and Blankschtein, 2003). Each of these contributions depends on the location and orientation of the surfactant molecules within the micelle. Intuitively, in a confined surfactant solution, the relative contributions of these physicochemical factors may be very different from those found in a bulk solution, mainly because of the external forces originated from the confining walls. The orientation of the surfactant molecules in a micelle may also be different because of their interactions with the walls. Consequently, g_{mic}, and therefore the free energy of formation, G_f, may differ considerably from those in a bulk solution.

1.5 Surfactant Adsorption on Solid Surfaces

As mentioned earlier, in a surfactant solution, the hydrophobicity of a surfactant tail induces structuring of the surrounding water molecules, which lowers the system entropy. As the surfactants begin to self-aggregate above the CMC, the release of these ordered water molecules results in an increase in system entropy, which is, in fact, the major driving force for micellization. In a confined surfactant solution, a similar effect can be found when surfactant molecules adsorb to the solid–liquid interface, thereby releasing the ordered water molecules around the surfactant tail (Tulpar and Ducker, 2004). Surfactant adsorption may play an important role in the self-assembly of surfactants in confined geometries, particularly when they are confined in a very narrow slit. As the surfactant concentration increases, the orientation of the adsorbed surfactant tails changes from parallel to perpendicular to a hydrophobic surface (Zettlemoyer, 1968). It is also possible to control the self-assembly of surfactants on the solid surface by altering the

solid–liquid adsorption process; thus, the anchored surfactant micelles may affect the properties of the interface (Yu *et al.*, 2003).

The behaviour of surfactants at a solid–liquid interface is affected by several factors, including electrostatic attraction, covalent bonding, hydrogen bonding, hydrophobic interaction, and solvation and desolvation of various species. The strength of these forces, which bind the surfactant molecules to the interface, depends on the characteristics of the solid surface and the surfactants (Somasundaran and Huang, 2000). The silica surface has been studied extensively since it is the major constituent of earth's crust (Iler, 1979). A considerable amount of research related to surfactant adsorption at the solid–liquid interface involves amorphous silica (Goloub *et al.*, 1996; Trompette *et al.*, 1994). Cationic surfactants with linear hydrocarbon chains form admicelles on silica substrates without any long-range ordering, because the electrostatically adsorbed monomers act as nucleation sites for further surfactant adsorption (Manne and Gaub, 1995; Velegol *et al.*, 2000). Grant *et al.* (2000) showed that the orientation of adsorbed surfactants changed with the hydrophobicity of the surface. In particular, they showed experimentally that hydrophobic force was the main driving force for the adsorption of ethylene oxide at a partially hydroxylated surface, and that hydrogen bonding reduced the free energy penalty by displacing water molecules. The interactions between surfactants and most hydrophilic surfaces are relatively weak, and water molecules can form hydrogen bonds with many sites on these surfaces, which allow them to compete for more surface area. As the hydrophobicity of the surface increases, the attraction between the surface and the surfactants becomes stronger; in addition, higher surface hydrophobicity also weakens the interactions between the surface and water molecules.

Graphite surfaces are widely used as substrates in atomic force microscopy (AFM) because of its ability to form atomically smooth crystalline structures (Atkin *et al.*, 2003). It has been observed in many AFM experiments that various types of surfactants (e.g., ionic, nonionic, and zwitterionic surfactants) with hydrocarbon tails longer than 12 carbon atoms form hemicylindrical micelles on graphite walls. However, with shorter tails, surfactants form featureless monolayer on graphite (Manne *et al.*, 1994; Manne and Gaub, 1995; Patrick *et al.*, 1997; Ducker and Grant, 1996). Thus, the

molecular structure of the confining wall may play a critical role in determining the self-assembling behaviour of a surfactant solution confined in a narrow slit.

1.6 Molecular Dynamics Simulation of Surfactant

Molecular dynamics (MD) simulation has become an increasingly powerful tool in the study of micellar systems because of its ability to probe the detailed structure of surfactant aggregates. Indeed, results of MD simulations have helped to advance the understanding of various phenomena observed in surfactant self-assembly. For example, Stephenson *et al.* (2006) used MD simulation to estimate the extent of hydration of surfactant head groups, hence enhanced the accuracy of the molecular-thermodynamic framework discussed in section 1.4. Bruce *et al.* (2002b) applied atomistic MD simulations successfully to investigate the structure of a sodium dodecyl sulfate (SDS) micelle, and Jorge (2008) reported the observation of micelle formation in the MD simulation of *n*-decyltrimethylammonium bromide.

Since the time scale of micelle formation is on the order of microsecond, and CMCs are usually in the range of 1–100 mmol, MD simulation of surfactant micellization tends to be computationally intensive. The issue of concentration is often overcome by selecting a surfactant which has a high CMC and low aggregation number. In addition, because of the limitation of computational power, older simulation studies often used concentrated surfactant solutions (several times higher than the CMC) in order to accommodate a sufficient number of surfactant molecules for micelle formation in a simulation cell. For instance, Bruce *et al.* (2002a) used a 0.4 M sodium dodecyl sulfate (SDS) solution, and Gao *et al.* (2005) considered SDS concentrations between 0.4 M and 1.1 M, which are well above the CMC of SDS in bulk solution. Both studies stated that the results were in qualitative agreement with experimental observations.

Different coarse-graining schemes have also been proposed to model surfactant solutions in an effort to reduce the simulation time required (Cheong and Panagiotopoulos, 2006; Davis and Panagiotopoulos, 2009; Sanders and Panagiotopoulos, 2010). Using lattice Monte Carlo simulation, Zhang *et al.* (2007) showed that the CMC

shift was affected by the presence of a confining boundary and by the wall–surfactant interactions. The mechanism of surfactant adsorption on hydrophobic and hydrophilic surface domains was studied by Reimer *et al.* (2001). They showed that the adsorption layers displayed a different behaviour for hydrophilic and hydrophobic surface domains. Using potentials of mean force (PMF) based on a coarse-grained model, Xu *et al.* (2008) evaluated the detailed thermodynamics of surfactant adsorption on solid–liquid interfaces. They revealed that, relative to solvent-philic surface, the solvent-phobic surface generated more stable sites for surfactant adsorption. Although these coarse-grained models or lattice MC simulations are useful in describing surfactant self-assembly qualitatively, they are not capable of revealing the details of surfactant aggregates. Some MD studies employed implicit treatment of water to make a large-scale simulation possible (Shinto *et al.*, 2004; Lazaridis *et al.,* 2005); however, experimental evidence has shown that chemical specificity of the intermolecular interactions between surfactant and water molecules cannot be ignored, because it plays an important role in controlling the phase behaviour and rheology of surfactant solutions (Pasquali, 2010; Ketner *et al.*, 2007).

Molecular dynamics simulations have also been used to better understand the phenomena of surfactant aggregation on solid–liquid interfaces at the molecular level (Dominquez *et al.*, 2006). In most atomistic MD studies of this kind, graphite wall is used as a hydrophobic adsorbate in aqueous media (Tummala and Striolo, 2008; Shah *et al.*, 2006), while silica wall is used as a typical hydrophilic adsorbate (Shah *et al.,* 2005). Using MD simulation, Shah *et al.* (2006) showed that hydrophilic and hydrophobic surfaces produced different effects on surface adsorption and on the morphology of the adsorbed cationic surfactant aggregates. In particular, surfactant monolayers and bilayers evolved into spherical structures on silica walls, but hemicylindrical structures on graphite walls. Tummala and Striolo (2008) and Tummala *et al.* (2010) also used MD simulation to study the morphology of SDS aggregates formed on graphite walls, and showed the effects of frontal and lateral confinement on surfactant adsorption. They reported that the morphology of the adsorbed aggregates was altered by the two graphite walls approaching each other with a separation distance less than 4.05 nm, although the fundamental reasons behind this observation were not fully explained. Nevertheless,

based on the results of these simulation studies, it is conceivable that hydrophilic and hydrophobic boundaries may also affect the morphology of surfactant aggregates formed under confinement, and atomistic MD simulations can be used to explore the behaviour of confined surfactant solutions.

1.7 Objectives

As stated earlier, there is still a lack of fundamental knowledge regarding the behaviour of confined surfactant solutions, and a more thorough understanding of these systems would advance the development of many novel technologies. The main objectives of this thesis are therefore to

(i) Explore the effects of confinement on surfactant micellization, particularly the morphology of micelles, and
(ii) Obtain some insight into surfactant self-assembly in these confined systems.

More specifically, a series of atomistic MD simulations was performed to study the behaviour of sodium octanoate (SO) solutions confined between two parallel walls. All the simulations in this study were designed to explore the system's response to changes in three important system parameters: surfactant concentration, gap size (distance between the two confining walls), and wall type. As discussed earlier, different types of walls contribute differently to the system behavior; thus, three types were selected for this purpose: (i) graphite wall, (ii) hydrophilic silica wall, and (iii) hydrophobic silica wall. The range of surfactant concentrations was selected so that micellization can be observed even after surfactant adsorption. It is worth noting that many previous atomistic MD studies of surfactant aggregates were performed on systems composed of pre-formed spherical or rodlike micelle (Maillet *et al.*, 1999; Bruce *et al.*, 2002a; de Moura and Freitas, 2005). This type of simulation assumes that the shape and aggregation number of the micelle do not deviate significantly from the initial configuration. In contrast, the initial configuration adopted in this study consists of surfactant monomers dispersed in water, and any micellization would occur spontaneously during the simulation.

The remainder of this thesis is organized as follows: Chapter 2 describes the methodology employed in this study, the simulation parameters, and the procedure used to develop the MD simulations and analyze the data. The results of a preliminary study designed to validate the simulation parameters are given in Chapter 3. Chapter 4 describes and discusses the results for SO solutions confined by graphite walls. In Chapter 5, the effects of hydrophobic and hydrophilic silica confinements are discussed, and finally concluding remarks are given in Chapter 6, along with some future research directions.

CHAPTER 2

METHODOLOGY

The general configuration of the system used in this study consists of an aqueous sodium octanoate (SO) solution confined by two parallel walls. The molecular structure of SO is shown in Figure 2.1. The distance between the two inner surfaces of the walls is referred to as gap size. The minimum gap size considered here is 3 nm, since it is known from other experimental studies that the radius of a spherical SO micelle at concentrations around the CMC is about 1.30 nm (Hayter and Zemb, 1982). The other gap sizes selected for this study are 4 nm, 5 nm, and 6 nm.

2.1 Simulation Model

Three types of confinement were considered in this study: (i) graphite wall, (ii) hydrophilic silica wall, and (iii) hydrophobic silica wall. Each graphite wall is composed of 2592 carbon atoms arranged in four graphene sheets (see Figure 2.2). The distance between two adjacent graphene sheets is 0.335 nm, and the *x–y* dimension of the graphite wall is 4.298 nm × 3.686 nm. The hydrophobic and hydrophilic silica walls were constructed based on the ideal beta cristobalite (C9) structure (NRL, 2010), following the method described by Giovambattista *et al.* (2006). Each hydrophobic wall has four layers of SiO_2, reproducing the (1.1.1) octahedral face of cristobalite. The unit cell of SiO_2 is idealized as a perfect tetrahedron with the O–O and Si–O distances of 0.247 nm and 0.151 nm, respectively. None of the atoms in the hydrophobic silica wall carry any partial charge; thus, these atoms interact with other atoms solely via the Lennard-Jones (LJ) potential, whose parameters were taken from the GROMOS96 force field ("G45a3"). Each hydrophobic silica wall has 1170 atoms, with a *x–y* dimension of 4.446 nm × 4.278 nm.

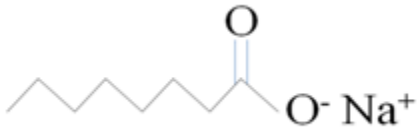

Figure 2.1: Molecular structure of sodium octanoate.

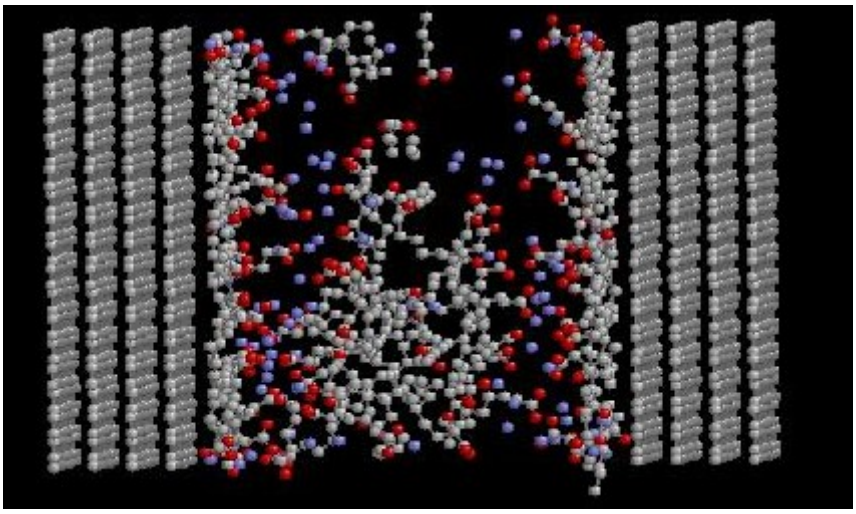

Figure 2.2: A snapshot depicting a sodium octanoate solution confined between two graphite walls.

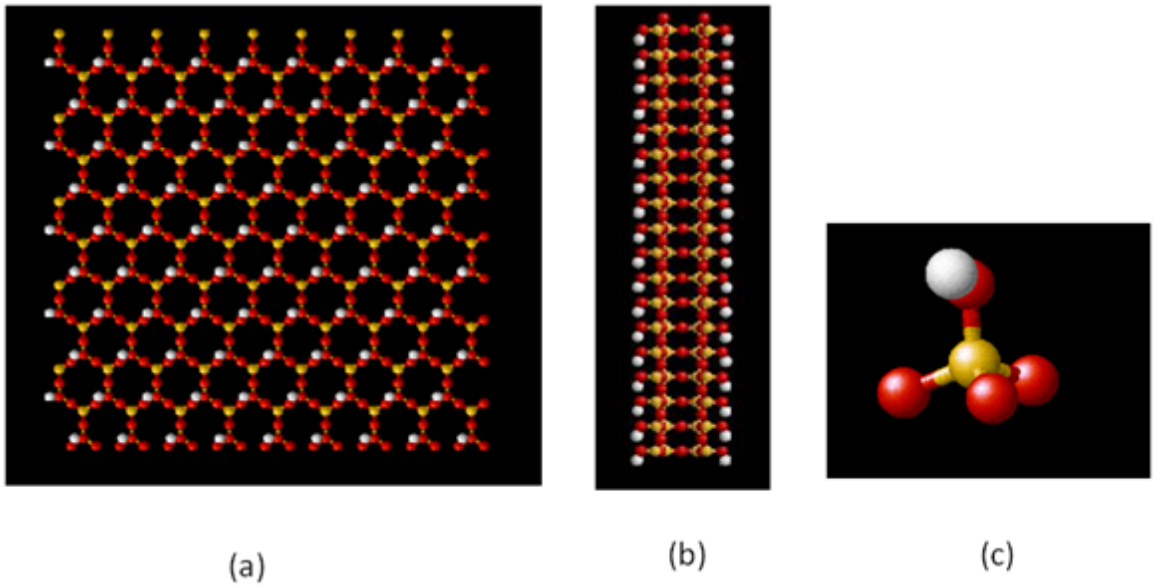

Figure 2.3: Snapshots of the hydrophilic silica wall showing (a) view of the *x*–*y* plane and (b) view of the *y*–*z* plane. (c) A SiO_4H unit. Red, yellow, and white spheres represent oxygen, silicon, and hydrogen atom, respectively.

The hydrophilic silica wall was constructed by attaching a hydrogen atom to each surface oxygen atom in the hydrophobic silica wall (see Figure 2.3). In this case, each surface Si–O–H group carries a partial charge, which is given in Table 2.1. The O–H bond length is 0.1 nm, the same as that in the simple point charge (SPC) water model. The positions of the Si and O atoms are fixed in both hydrophobic and hydrophilic silica walls, but in the hydrophilic wall, the H atoms on the surface are allowed to move with fixed bond length and angle. The Si–O–H bond angle is set at 109.27^{o} so that the H atom moves on a plane that is 0.033 nm away from the surface O-atom plane of the Si–O–H group. Each hydrophilic silica wall contains 1350 atoms.

2.2 Simulation Procedure

The MD simulation package, GROMACS (version 4.0), was used to perform all the simulations in this study (Berendsen, 1995; Hess *et al.*, 2008). The GROMOS96

Table 2.1: Charges on the surface Si–O–H group of the hydrophilic silica wall.

Atom type	Charge (*e*)
O	–0.71
Si	0.31
H	0.40

("G45a3") force field was selected for use with the SPC water model. Although this force field and water model have been used previously to study the micellar behaviour of bulk SO solutions (Schuler *et al.*, 2001; Berendsen, *et al.*, 1981), a series of simulations was performed in this study to validate the selected set of parameters (see Chapter 3).

The molecular topology of the octanoate ion was generated using the PRODRG algorithm with the GROMOS96 force field (Schuttelkopf and van Alten, 2004). The initial configuration of the central simulation cell was built by arranging the octanoate ions in a cubic lattice between the walls. The Na^+ ions were then distributed randomly, and the remaining space between the two walls was filled with water molecules using the `spc216.gro` file provided with the GROMACS package so that the liquid density was approximately 997 g/L.

All bonds in the octanoate ion and water molecule were constrained by the LINCS and SETTLE algorithms, respectively (Allen and Tildesley, 1987). All the wall atoms, except the H atoms in the hydrophilic wall, were fixed in space. The *x*–*y* dimension of the simulation cell is the same as that of the walls. Periodic boundary conditions were imposed in all three directions. However, a vacuum of 10 nm was added to each side beyond the wall in the *z*-direction to minimize the influence of the molecules in adjacent simulation cells in the same direction.

The particle-mesh Ewald (PME) method was used to account for the long-range electrostatic interactions. Before each simulation, the steepest descent method was used to minimize the energy of the initial configuration to a maximum force of 60 kJ/mol nm. After energy minimization, simulations were performed in the *NVT* ensemble with a time step of 2 fs. The temperature was kept constant at 298 K using the Berendsen thermostat (Berendsen *et al.*, 1984), with a time constant of 0.02 ps. The Berendsen thermostat has

been used widely because of its stability and efficiency (D'Alessandro *et al.*, 2002; Morishita, 2000). The cut-off distances for the real part of the Coulombic potential and the LJ potential were set at 0.9 nm and 1.5 nm, respectively. Note that the GROMOS96 force field was parametrized based on a LJ cut-off distance of 1.4 nm (van der Spoel *et al.*, 2005).

In a previous MD simulation study of aqueous SO solutions, de Moura and Freitas (2005) showed that spontaneous formation of micelles from monomers occurred within 20 ns. However, in the present study, a preliminary set of simulations had revealed that the self-aggregation of SO in water might take as long as 60 ns. Thus, all the simulations in this study were equilibrated for at least 80 ns, and the data from the additional 20 ns–40 ns were used for analyses.

2.3 Potential of Mean Force

As discussed in Chapter 1, the self-assembly of ionic surfactants is governed by various interactions between the surfactant molecules, including electrostatic interactions and van der Waals attractions. In confined geometries, these intermolecular interactions may be altered by the presence of the confining walls. To assess the possible effects of the external boundaries on intermolecular interactions, the potential of mean force (PMF) between different atomic groups was determined using the constrained MD technique (Ciccotti *et al.*, 1989) as described by Shinto *et al.* (2003). Potential of mean force is the interaction between two particles (molecules or groups of atoms) constrained at a fixed separation distance when the remaining molecules of the system are canonically averaged over all configurations (McQuarrie, 1973). It has been used in previous studies to elucidate the microscopic mechanisms of the surfactant adsorption process (Striolo and Prausnitz, 2001; Xu *et al.*, 2008).

In this study, the mean force, $F(r)$, between two groups of solute atoms separated by a distance r was determined by performing a series of MD simulations with different values of r, which was kept constant in each simulation. The PMF, $W(r)$, was then obtained by integrating the mean force, i.e.,

$$W(r) = W(r_0) - \int_{r_0}^{r} F(r)\, dr \qquad (2.1)$$

where $W(r_0)$ is the PMF at a sufficiently large separation r_0, and was taken to be the Coulombic potential, i.e.,

$$W(r_0) = \frac{1}{4\pi\varepsilon_r\varepsilon_0}\frac{q_a q_b}{r_0} \qquad (2.2)$$

where q_a and q_b are the charges of the two groups of atoms, $\varepsilon_r = 78.5$ is the relative permittivity of water, and $\varepsilon_0 = 8.854 \times 10^{-12}$ C^2/N m^2 is the permittivity in vacuum. The value of r_0 was set at 1.1 nm and the integration in eq 2.1 was performed numerically using the integration routines provided in the Gnu Scientific Library (GNU, 2010). The separation between the two groups of atoms was varied from 0.22 nm to 1.10 nm, with an increment of 0.02 nm. For ionic pairs, the separation range was 0.30 nm–0.70 nm, with an increment of 0.01 nm.

The procedure and simulation parameters used in each constrained simulation were the same as those described in section 2.2, except that a smaller simulation cell was used. The *x*–*y* dimension of the graphite wall in this case is 3.686 nm × 2.825 nm, whereas that for the hydrophilic and hydrophobic silica wall is 3.50 nm × 3.00 nm. For PMFs in a bulk solution, a cubic box with a volume of 27 nm^3 was used. The simulation time for each separation distance was 8 ns, in which the initial 1 ns was used as equilibration. The time-average of the forces obtained from the 7-ns production run was used in the integration (see eq 2.1). To determine the PMF between a confining wall and a group of atoms or molecule, the water molecules were used as the reference group, and the distance *r* was measured from the center of mass (COM) of the water molecules. Thus, *r* increases as the atom group or molecule approaches the wall.

2.4 Aggregate Size Determination

The approach of Shinto *et al.* (2004) was adopted in this study to determine if a surfactant molecule belongs to an aggregate or cluster. A cut-off distance of 0.48 nm was used in this cluster analysis, since it was found that, with SPC water, the PMF between two

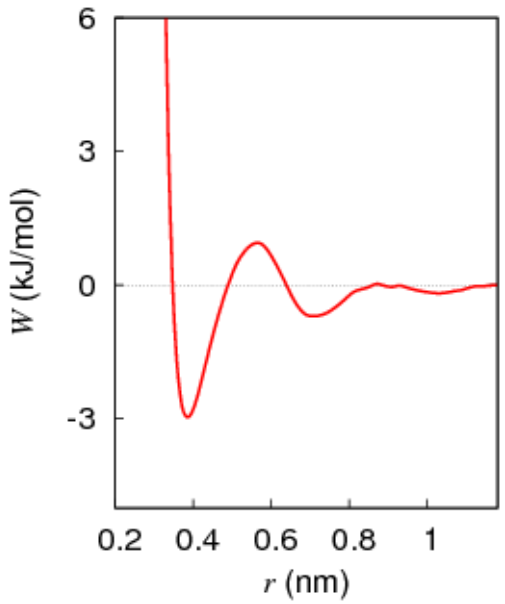

Figure 2.4: Potential of mean force of a methane–methane pair in ambient water (SPC).

methane molecules is zero at this separation distance, after the energy minimum located at approximately 0.4 nm (see Figure 2.4). Accordingly, if any methylene or methyl group of an octanoate ion lies within the cut-off distance of a methylene or methyl group of another octanoate ion, they are considered to be in the same cluster. To determine the cluster or aggregate sizes in confined surfactant solutions, the **g_clustsize** utility program supplied with GROMACS was modified to account for the adsorbed surfactant molecules.

2.5 Surfactant Adsorption

Surfactant adsorption to the confining walls was determined by considering the perpendicular distance between the wall and any atomic group of a surfactant molecule. If this distance is smaller than a distance r_{min}, the surfactant molecule is treated as an adsorbed molecule. The value of r_{min} was taken as 0.52 nm, based on the PMF between a methane molecule and the graphite wall (see Figure 2.5). At this distance, the PMF

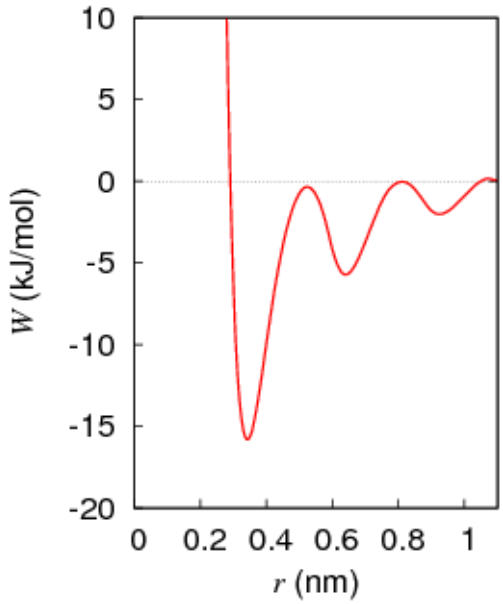

Figure 2.5: Potential of mean force between a methane molecule and the graphite wall. A methane molecule is confined by two parallel graphite walls with a gap size of 4 nm. The methane molecule is pulled from the center of mass of the confined water molecules.

reaches a local maximum of approximately zero, after the global energy minimum located at 0.35 nm.

2.6 Density Distribution

The **g_density** utility program supplied with GROMACS was used to determine the density profile of atoms or molecules as a function of the *z*-coordinate across the gap. The density profile was calculated by dividing the simulation cell into thin layers parallel to the wall, each with a width of 0.01 nm.

The density distribution of selected atoms and water molecules around the COM of a micelle was also determined to characterize the micellar morphology. This radial density distribution was calculated by counting the number of atoms or atomic segments within layers of spherical shells, each having a width of 0.03 nm, around the COM of a micelle.

2.7 Radial Distribution Function

The radial distribution function, $g(r)$, was determined using the histogram approach outlined by Allen and Tiledesley (1987). More specifically, the function can be calculated as

$$g(r) = \frac{n_{\text{his}}(b)/(N \times \tau_{\text{run}})}{\frac{4}{3}\pi\rho[(r+\delta r)^3 - r^3]} \tag{2.3}$$

where $n_{\text{his}}(b)$ represents the number of particles in the b-th bin of the histogram, N is the number of particles considered, τ_{run} is the number of time frames used in the analysis, r is the distance between two particles, ρ is the number density, and δr is the bin width, taken as 0.01 nm. Equation 2.3 is applicable to a bulk solution where spherical symmetry exists. In case of a confined solution, because of the presence of the confining boundaries, spherical symmetry is valid only for a small volume around each particle, and therefore eq 2.3 must be applied with care. Nevertheless, this equation has been used in previous studies to describe liquid structures in both bulk solutions and the vicinity of an interface (Tummala and Striolo, 2008).

2.8 Water Structure

The orientation of a water molecule was characterized in this study by the angle θ_{OH}, which is the angle between the O–H bond of a water molecule and the inward normal to the wall (see Figure 2.6). The probability distribution of this angle, $P(\theta_{OH})$, has been used as a measure of surface hydrophobicity (Lee *et al.*,1984; Giovambattista *et al.*, 2007; Giovambattista *et al.*, 2009). For hydrophilic surfaces, the value of $P(\theta_{OH})$ tends to be large at $\theta_{OH} = 0$, whereas for hydrophobic surfaces, $P(\theta_{OH})$ is large at $\theta_{OH} = 180^o$ (Giovambattista *et al*., 2006). Note that $P(\theta_{OH})$ was corrected for the solid angle bias.

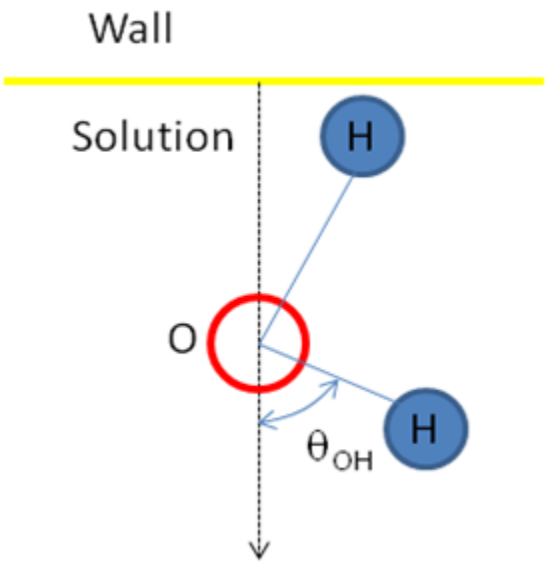

Figure 2.6: Schematic diagram depicting the angle θ_{OH} formed between the O–H bond of a water molecule and the outward normal to the wall.

CHAPTER 3

SIMULATION OF BULK SODIUM OCTANOATE SOLUTIONS AND CHARACTERIZATION OF THE WALLS

3.1 Introduction

As stated in Chapter 2, the GROMOS96 ("G45a3") force field and the SPC water model were used to study the self-assembling behaviour of confined surfactant solutions. Although this force field and water model have been used in previous simulation studies (Hu and Jiang, 2010; Gandhi and Mancera, 2010), it is critical to assess the applicability of the selected simulation parameters, particularly their ability to predict the self-assembling behaviour of surfactants. Unfortunately, to the best of our knowledge, no experimental data are available for SO solutions confined in a nanometer-scale space. In light of this limitation, a bulk SO solution was used as an alternative for this validation step. More specifically, our primary objective is to verify the validity of the selected force field and water model in simulating the behaviour of SO in water, particularly their ability to capture the salient features of the self-assembling behaviour of the SO surfactant. Although the overall behaviour of a confined surfactant solution may be different from that of a bulk solution because of the presence of the confining walls, the underlying intermolecular and intramolecular interactions should remain the same. Consequently, the simulation parameters which are capable of describing bulk surfactant solutions should, in principle, be able to provide an accurate description of the confined systems.

In addition to validating the simulation parameters, this chapter also describes the characterization of the three types of walls considered in this study. In particular, the hydrophobicity of each type of wall was characterized based on the orientation of the water molecules adjacent to the wall. Such a characterization will not only provide a

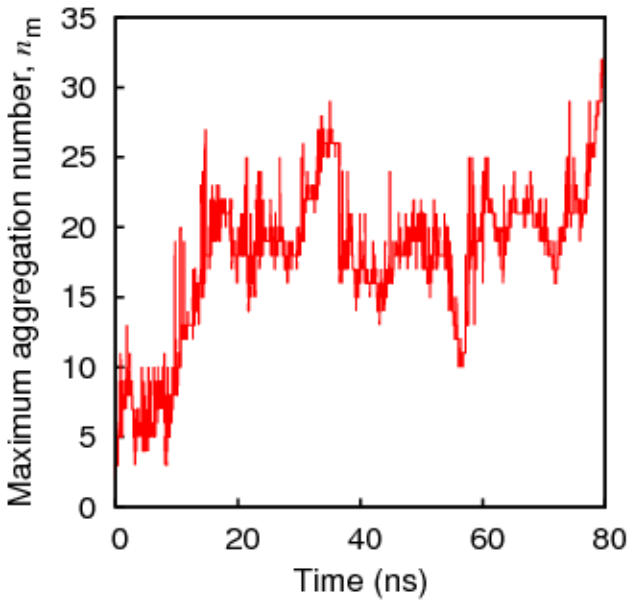

Figure 3.1: Simulated time variation of maximum aggregation number, n_m, in a 0.55 M sodium octanoate solution.

more quantitative description of the nature of the walls, but also facilitate the understanding of the simulation results discussed in Chapters 4 and 5.

3.2 Micelle Formation in Sodium Octanoate Solutions

Figure 3.1 depicts the time evolution of the maximum aggregation number, n_m, in a 0.55 M SO solution. As shown in the figure, n_m fluctuates between 5 and 10 in the first 10 ns, and large aggregates begin to appear at about 15 ns. The time-average of n_m between 60 ns and 80 ns is approximately 21, which is close to the experimental value of 18 measured using the light scattering technique (Zemb, 1983). The largest aggregate between 60 ns and 80 ns appears as spherical micelle. The shape of this micelle is reflected by its moments of inertia, where the ratio $\langle I_{xx}/I_{yy}\rangle/\langle I_{zz}/I_{yy}\rangle$ was found to be 0.87 (a perfect sphere would have a ratio of unity). Here I_{kk} denotes the moment of inertia around the k-axis (k denotes x, y, and z) through the center of mass of the aggregate, and the average is taken over all time frames between 60 ns and 80 ns of the simulation.

The density distributions of water, Na^+, and various atomic groups of the octanoate molecule from the center of mass (COM) of the largest aggregate are shown in Figure 3.2. The density profiles are qualitatively similar to those found in a spherical SDS micelle (Bruce, 2002b). Note that while the center of the aggregate ($0 < r < 0.4$ nm) is almost completely devoid of water, part of the hydrocarbon core (0.6 nm $< r <$ 1.15 nm) is in some contact with water. The density profile of the oxygen atoms displays a peak at approximately 1.15 nm, which is in agreement with many previous experimental works as summarized by de Moura and Freitas (2005).

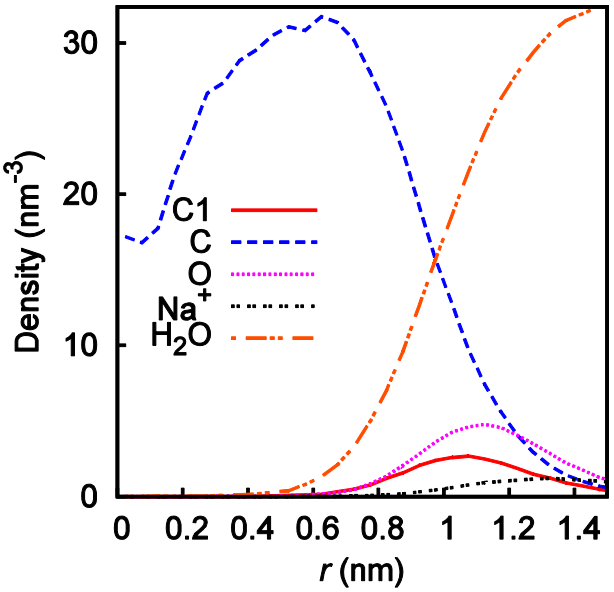

Figure 3.2: Average number densities of water (H_2O), counterion (Na^+), and various atomic groups of the octanoate molecule in a 0.55 M sodium octanoate solution. The distance r is measured from the center of mass of the aggregate. The average is taken from 60 ns to 80 ns. C denotes the methylene groups of the octanoate tail, C1 denotes the carbon atom attached to the oxygen atoms, and O denotes the oxygen atoms of octanoate.

3.3 Critical Micelle Concentration

One of the most characteristic features of a surfactant solution is the formation of micelles beyond the critical micelle concentration (CMC). Sammalkorpi *et al.* (2011) determined the CMC of sodium hexyl sulfate in water to be 0.25 M using atomistic MD simulation. They defined the CMC as the total concentration of oligomers present at equilibrium with the aggregates, following the approach of Floriano *et al.* (1999). However, this simulated value does not agree well with the experimentally measured value of 0.42 M (Rassing, 1974). In the present study, to determine the CMC of bulk SO solutions, we took the more tedious approach by performing a series of *NVT* simulations at five different concentrations around the CMC, and tracking the evolution of n_m with simulation time in each case. Figure 3.3 depicts the time variation of n_m for the five cases. With concentrations of 0.38 M and 0.41 M, the values of n_m still fluctuate around 5 between 60 ns and 80 ns. However, at concentrations equal to or higher than 0.46 M, large aggregates begin to appear within the same time period. Consequently, using the GROMOS96 force field with the SPC water model, these simulation results indicate that

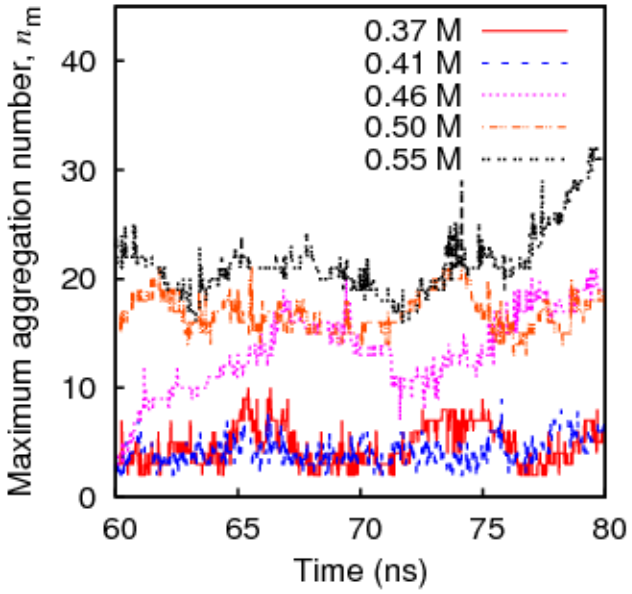

Figure 3.3: Simulated time variation of maximum aggregation number, n_m, in bulk sodium octanoate solutions at various concentrations between 0.37 M and 0.55 M.

the CMC of SO in water should lie between 0.41 M and 0.46 M, which is consistent with the experimental value of 0.4 M (Picquart, 1992; Kuhn *et al*, 1998; Gonzalez-Perez *et al.*, 2003).

3.4 Characterization of Confining Walls

The orientation of water molecules was studied following the approach of Lee and McCammon (1984), which has also been used successfully by other researchers (Giovambattista *et al.*, 2007; Layfield and Troya, 2011) to characterize the nature of solid surfaces. To assess the hydrophobicty of the three types of walls considered in this study (graphite, hydrophilic silica, and hydrophobic silica), three separate simulations were performed in which only water was confined in a 4-nm gap. The average density distributions of water near the wall are shown in Figure 3.4. For the hydrophilic silica

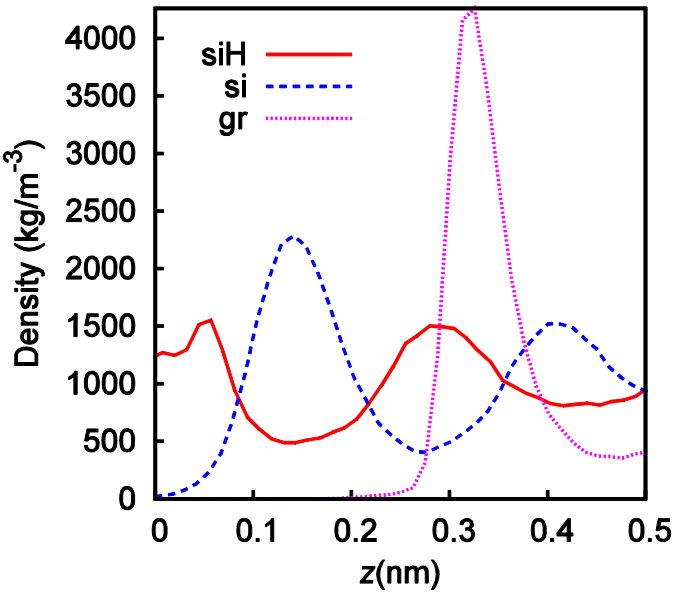

Figure 3.4: Density profiles of water along the *z*-axis. Pure water is confined by two parallel walls (siH: hydrophilic silica, si: hydrophobic silica, gr: graphite) with a gap size of 4 nm. Here *z* represents the distance from the inner surface of the wall. For the hydrophobic silica wall, the inner surface is located at the plane of the surface O atoms, whereas for the hydrophilic silica wall, the plane of the surface H atoms is considered as the inner surface.

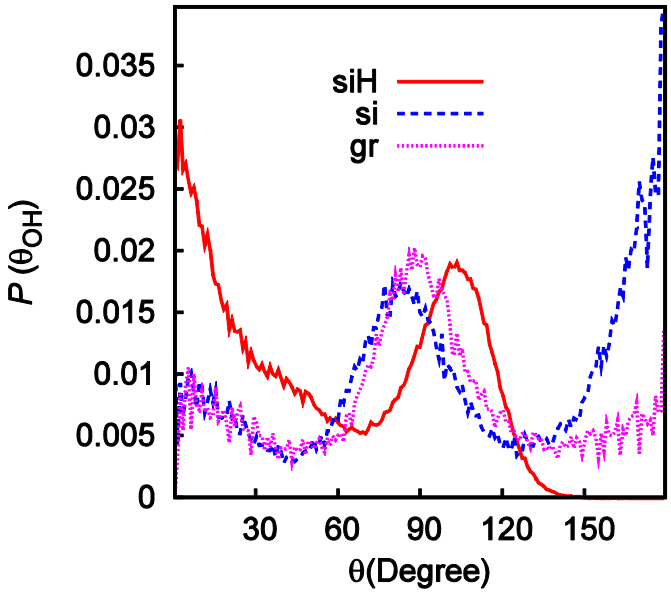

Figure 3.5: Probability distribution, $P(\theta_{OH})$, of angle θ_{OH} between hydrogen bond vectors of water molecules and the normal direction to the plates, for molecules at a distance ≤0.1 nm in case of hydrophilic and hydrophobic silica wall and ≤0.30 for graphite wall. Water is confined by two parallel walls with a gap size of 4 nm. Legends represent the types of wall.

wall, water molecules can be found very close to wall, which is due to the fact that water molecules actually enter the surface pockets around the O–H bonds. In the case of graphite confinement, water has the highest density at 0.32 nm away from the wall, mainly because of excluded volume effect. These density distributions help to determine the locations of the water film in which the orientation of the water molecules can be used to characterize the wall hydrophobicity.

The probability distributions, $P(\theta_{OH})$, of the angle θ_{OH} between the O–H bonds and the inward normal (see Chapter 2) for the water molecules in the water film adjacent to the wall are shown in Figure 3.5. In the cases of hydrophilic and hydrophobic silica walls, only those water molecules that are located within 0.1 nm from the plane of the surface H atoms and O atoms, respectively, were used in the calculation of $P(\theta_{OH})$. Note that in the hydrophilic silica case, $P(\theta_{OH})$ has its maximum value at close to zero degree and is almost zero at 180^{o}. Since the surface atoms of the hydrophilic silica wall possess

partial charges, they induce an attractive force between the wall and the water oxygen atoms. Consequently, the hydrogen bonds formed between the hydrophilic silica wall and the water molecules near the wall help to align the O–H bonds, with one pointing directly into the liquid phase and the other forming an angle of approximately 110^{o} with the inward normal. In contrast, in the hydrophobic silica case, the O–H bonds are mostly pointing into the wall as the maximum value is found at 180^{o}. For the graphite wall, only those water molecules that are located within 0.3 nm from the innermost wall atoms were used in the calculation of $P(\theta_{OH})$. As shown in Figure 3.5, most water molecules adjacent to the graphite wall tend to lie parallel to the wall, which suggests that the graphite wall is less hydrophobic than the hydrophobic silica wall

3.5 Concluding Remarks

Using the GROMOS96 (G45a3) force field with the SPC water model, the simulation results show that spherical micelles, with an aggregation number of 21 and a radius of approximately 1.15 nm, form spontaneously from monomers in a 0.55 M aqueous SO solution. The simulation also predicts a CMC value between 0.41 M and 0.46 M, in good agreement with experimental observations. This simulation study thus demonstrates the ability of the selected force field and water model to satisfactorily capture the salient features of the self-assembling process of SO in bulk solution. As stated earlier, since the same underlying interactions are involved in the simulation of confined surfactant solutions, it is reasonable to expect that the results presented in this study accurately reflect the behaviour of confined SO solutions. In addition, the characterization study has shown that the three types of walls considered here display different degree of hydrophobicity, which, as will be detailed in Chapters 4 and 5, would interact differently with the confined SO solutions, including the surfactant and the water molecules.

CHAPTER 4

SODIUM OCTANOATE CONFINED BY TWO PARALLEL GRAPHITE WALLS

4.1 Introduction

This chapter discusses the behaviour of SO solutions confined between two parallel graphite walls. More specifically, a series of constant-*NVT* MD simulations of SO solutions confined between two parallel graphite walls with gap sizes of 3, 4, and 5 nm was performed for 100 ns. The ranges of surfactant concentrations considered in these studies are given in Table 4.1. These concentration ranges were selected to allow for the observation of micelle formation within the different gap sizes. The results of these studies have revealed that, at lower concentrations, the octanoate molecules tend to adsorb on the graphite walls, but they start to form micellar aggregates at higher concentrations, after the walls are densely covered with surfactants. Formation of spherical micelles was observed in the 4-nm and 5-nm gaps but not in the 3-nm gap. In addition, as the surfactant concentration increases, the shape of the micelle also changes.

4.2 Micelle Formation in Confinement

Before discussing the effects of gap size and surfactant concentration, let us first consider a representative case in which a 2.1 M SO solution is confined within a 4-nm gap. Such a case would reveal the typical features of a SO solution confined between two graphite walls. Figure 4.1 depicts the density profiles of the two oxygen atoms (O), the first carbon atom (C1), i.e., the one attached to the oxygen atoms of the octanoate molecule, the last carbon atoms (C8), i.e., the end of the octanoate tail, counterions (Na^+), and water molecules (H_2O) in the z-direction (normal to the wall–solution interface). The centers of the innermost layers of wall atoms are located at $z = 0$ and $z = 4$ nm.

Table 4.1: Gap sizes and concentration ranges for the simulation studies of sodium octanoate solutions confined between two parallel graphite walls.

Gap size (nm)	Number of cases	Concentration range (M)
3	4	2–3.5
4	6	1.8–2.5
5	4	1.7–1.9

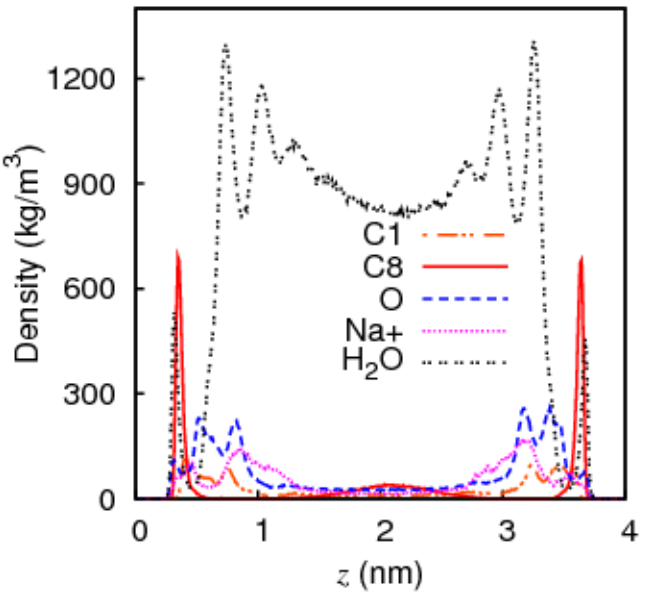

Figure 4.1: Density profiles of water (H_2O), counterion (Na^+), and various atomic groups of the octanoate molecule along the *z*-axis. A 2.1 M sodium octanoate solution is confined between two parallel graphite walls with a gap size of 4 nm. O, C1, and C8 denotes the oxygen atoms, the first carbon atom (attached to the oxygen atoms), and the last carbon atom of the octanoate molecule, respectively.

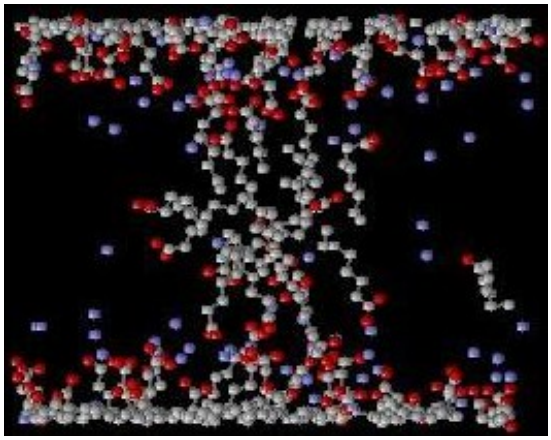

Figure 4.2: Snapshot of a 2.1 M sodium octanoate solution confined between two graphite walls, located above and below the solution layer, with a gap size of 4 nm (after 80 ns of simulation). The gray, red, and blue spheres represent carbon, oxygen, and Na^+, respectively. Water molecules and the two graphite walls have been removed for clarity.

As shown in Figure 4.1, the oxygen atoms (blue dashed line) are distributed within a region of approximately 0.9 nm from the walls, and a sharp peak in the C8 profile (red solid line) is found at about 0.38 nm from each wall. On the other hand, the densities of the oxygen atoms and the C1 atom (red dash-dotted line) in the central region of the gap are relatively low. This indicates that most octanoate molecules form an adsorbed layer spanning from the wall surface to about 0.9 nm away, with their end attached to the walls. The density profiles of the oxygen atoms and the C1 atom display various peaks within this adsorbed layer, suggesting that the octanoate molecules are forming different angles with the wall. A small peak of about 450 kg/m^3 in the water density profile (black dashed line) is also found next to the wall. These water molecules are probably associated with the few surfactant heads lying on the graphite wall surface. The density distributions depicted in Figure 4.1 are consistent with those obtained by Tummala and Striolo. (2008), Dominguez (2007), and Bandyopadhyay *et al.* (1998).

Although most octanoate molecules are adsorbed to the walls, the small, broad peak in the C8 profile at the mid-plane (z = 2 nm) suggests that some octanoate molecules are not adsorbed. In fact, these molecules form an aggregate between the two adsorbed layers. As shown in Figure 4.2, a snapshot taken at 80 ns clearly shows surfactant aggregation within the confinement. Figure 4.3 depicts the time-averaged density

distributions of Na^+, water, and various atomic groups of the octanoate molecule from the center of mass (COM) of the aggregate. These density profiles are typical of spherical micelles, thus providing secondary evidence for the formation of spherical aggregates within the confinement. Note that these density profiles are similar, at least qualitatively, to those observed in a bulk SO solution discussed in Chapter 3 (see Figure 3.2). However, in the bulk solution, no water penetration is observed, as the water density is almost zero within 0.6 nm from the COM of the micelle. In contrast, in the confined case, the density profile of water (see Figure 4.3) indicates that water is present near the micelle core, which suggests that the micelle is not very tight in the confined case. There is also a small finite density of C1 and O atom towards the center of micelle which also suggest that all the octanoate tails are not well arranged in the micelle.

4.3 Effect of Surfactant Concentration on Adsorption

As discussed in the preceding section, in a 2.1 M SO solution confined between a 4-nm gap, most of the surfactant molecules are adsorbed on the walls. Indeed, the same phenomenon was observed with other surfactant concentrations. Figure 4.4 depicts the density profiles of the C8 atom along the *z*-axis for different surfactant concentrations within a 4-nm gap. In all cases, a sharp peak in the density profile occurs at 0.38 nm away from the wall. This behaviour is consistent with the interactions between the graphite wall and the octanoate anions. As shown in Figure 4.5, the PMF between the graphite wall and an octanoate anion has its minimum located at 0.38 nm, indicating that the octanoate anion would tend to stay at this particular distance from the wall. Figure 4.4 also shows that as the surfactant concentration increases from 1.8 M to 2.5 M, the density of the C8 atom along the mid-plane increases, while the number of adsorbed molecules remains more or less constant, as shown in Table 4.2. In other words, within the concentration range considered here, the wall surface may have already been saturated with surfactants. Consequently, as the surfactant concentration increases, more octanoate molecules accumulate in the middle of the gap and form larger aggregates (see Table 4.2).

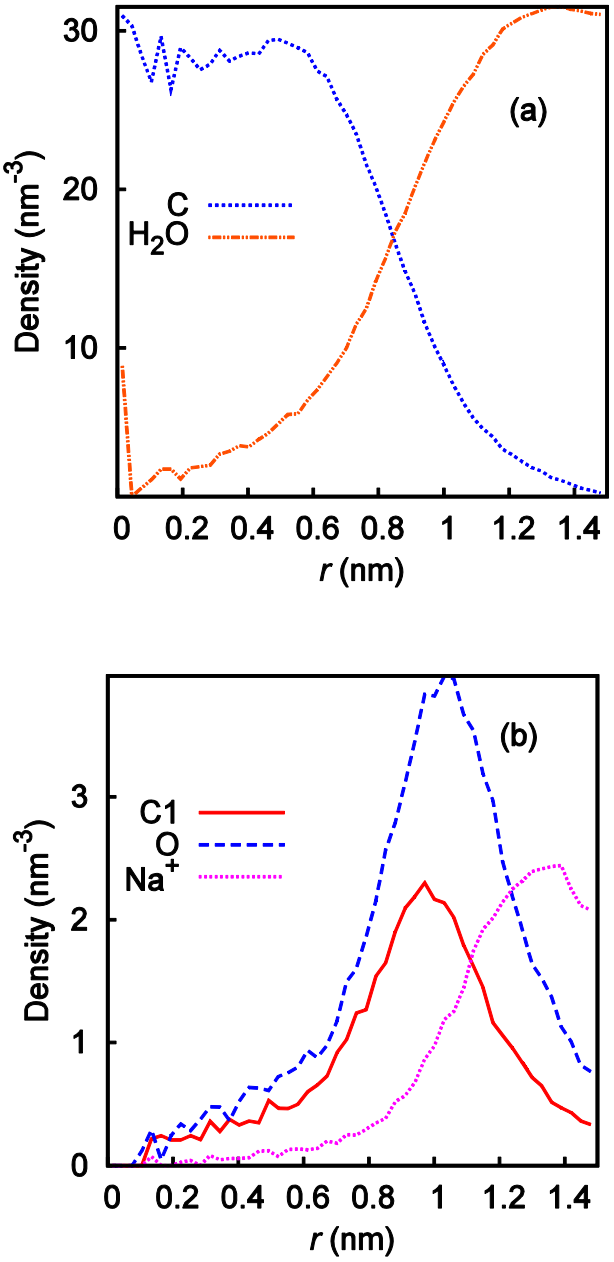

Figure 4.3: Average number density distributions from the center of mass ($r = 0$) of the largest aggregate formed between two parallel graphite walls (gap size = 4 nm). The concentration of the confined sodium octanoate solution is 2.1 M. (a) C and H_2O denote the carbon atoms of the octanoate molecule and water, respectively. (b) C1 and O denote the first carbon atom (attached to the oxygen atoms) and the oxygen atoms of the octanoate molecule, respectively. Na^+ represents the counterion.

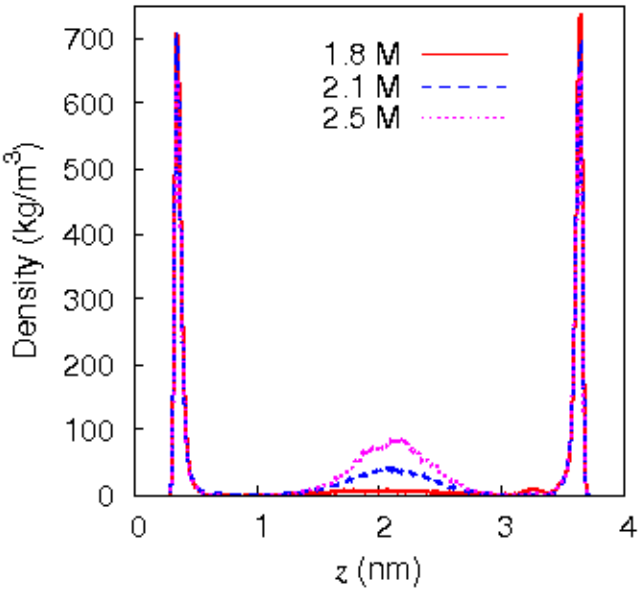

Figure 4.4: Density profiles of the C8 atom (end of surfactant tail) of the octanoate molecule for different surfactant concentrations. The SO solutions are confined between two parallel graphite walls with a gap size of 4 nm.

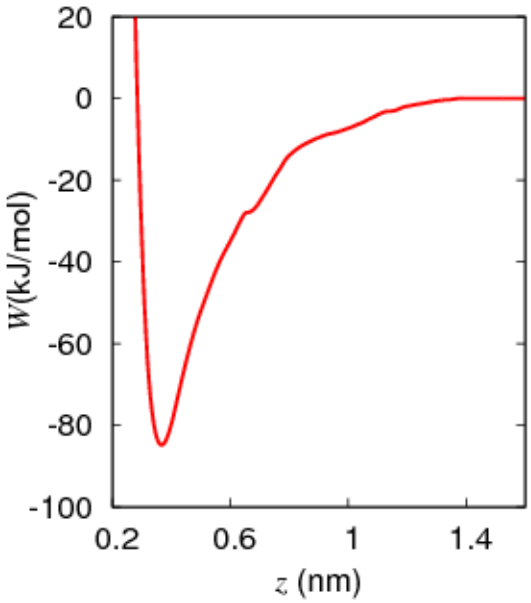

Figure 4.5: Potential of mean force between an octanoate anion and graphite wall. An octanoate anion and a Na^+ counterion are confined by two parallel graphite walls with a gap size of 4 nm. The octanoate anion is pulled from the center of mass of the confined water molecules.

Table 4.2: Surfactant adsorption and aggregate size variation in sodium octanoate (SO) solutions confined between two parallel graphite walls with a gap size of 4 nm.

Number of SO molecules in simulation cell	Overall concentration (M)	Number of adsorbed molecules	Average of maximum aggregation number
68	1.8	62	2
72	1.9	56	11
76	2.0	61	11
80	2.1	60	17
88	2.3	59	24
96	2.5	57	38

4.4 Effect of Concentration on Micelle Size

As shown in Table 4.2, the size of the aggregate found in the 4-nm gap increases with increasing surfactant concentration. Indeed, the maximum aggregation number of 24 at a concentration of 2.3 M is about double that at 1.9 M. To discern the differences between these aggregates, the distributions of Na^+, water, C1 atom, oxygen atoms, and the surfactant tail atoms around the COM of the aggregate are plotted in Figure 4.6 for the two cases: 1.9 M and 2.3 M. Taking the peak distance of the oxygen atoms from the COM as the radius of the aggregate, it can be seen readily that the aggregate in the 2.3 M solution has a larger radius (1.1 nm) than that in the 1.9 M solution (0.9 nm). Moreover, the core of the aggregate found in the 2.3 M solution appears to contain some water, which is similar to that found in the 2.1 M solution (see Section 4.2). On the other hand, the core of the aggregate found in the 1.9 M solution is rather dry with negligible water penetration.

Figure 4.7 depicts the density profiles of the oxygen atoms for four surfactant concentrations. Note that the aggregate radii in the 2.1 M and 2.3 M solutions are quite similar. However, at a higher concentration of 2.5 M, where the aggregation number reaches a value of 38 (see Table 4.2), an elongated aggregate was observed. The non-

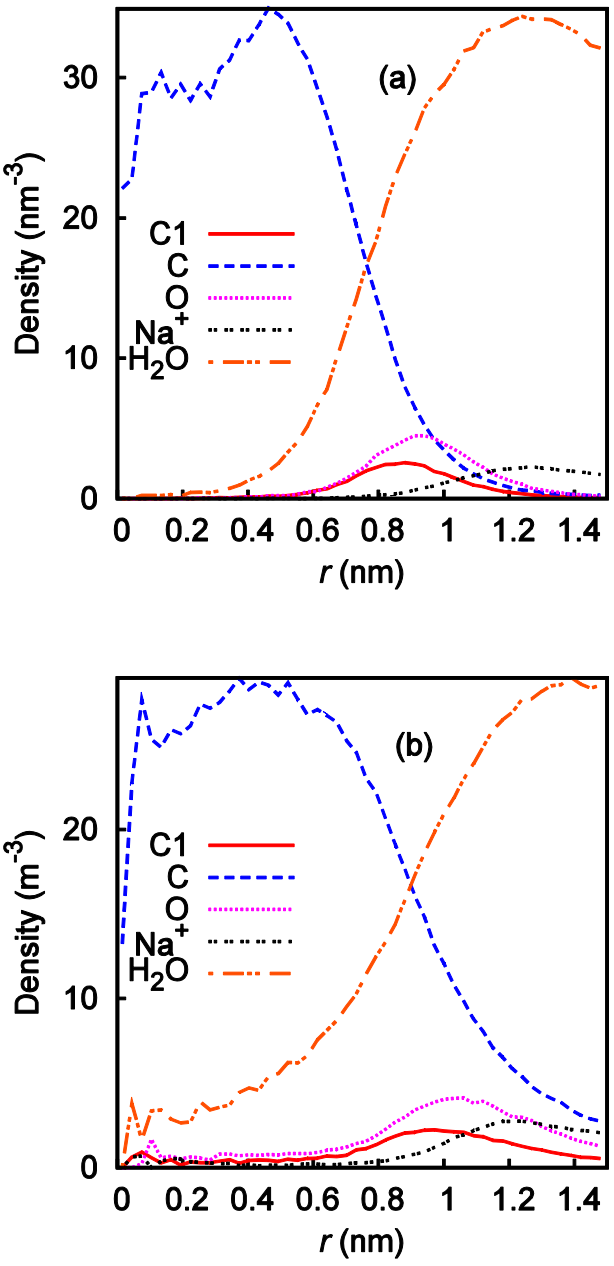

Figure 4.6: Average number density distributions from the center of mass ($r = 0$) of the largest aggregate formed between two walls with a gap size of 4 nm. The concentrations of the confined sodium octanoate solution are (a) 1.9 M and (b) 2.3 M. C and H_2O denote the carbon atoms of the octanoate molecule and water, respectively. C1 and O denote the first carbon atom (attached to the oxygen atoms) and the oxygen atoms of the octanoate molecule, respectively. Na^+ represents the counterion.

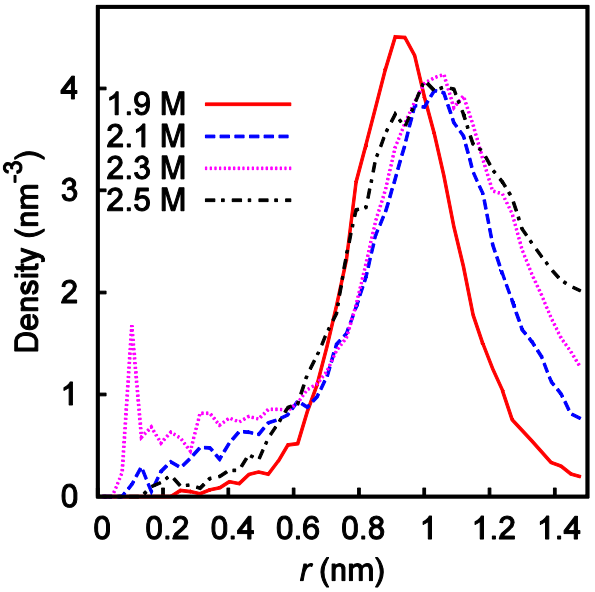

Figure 4.7: Average number density distributions of the oxygen atoms from the center of mass ($r = 0$) of the largest aggregate formed between two walls with a gap size of 4 nm. The labels are the surfactant concentrations of the confined sodium octanoate solutions.

spherical shape of this aggregate is reflected by its moments of inertia. More specifically, the ratio $\langle I_{xx}/I_{yy}\rangle/\langle I_{zz}/I_{yy}\rangle$ is plotted against the surfactant concentration in Figure 4.8. Here I_{kk} denotes the moment of inertia around the k-axis (k denotes x, y, and z) through the center of mass of the aggregate, and the average is taken over the aggregates that formed in each frame between 80 ns and 100 ns of the simulation. Note that a ratio of unity means that the aggregate is a perfect sphere. Thus, in the 4-nm gap, the aggregate is more or less spherical when the surfactant concentration is between 1.9 M and 2.3 M, as the ratios are close to 1. At 2.5 M, however, the aggregate shape deviates considerably from a sphere, since the ratio is much lower than 1. Indeed, such a change in shape is associated with an increase in aggregation number (see Table 4.2). Similar behaviour was also observed with the 5-nm gap, i.e., the aggregate size increases with increasing surfactant concentration (see Table 4.3), although the concentrations were varied only within a narrow range (1.67 M–1.92 M) compared to those in the 4-nm gap case. These aggregates are also approximately spherical, as their ratios of moment of inertia are close to unity (see Figure 4.8).

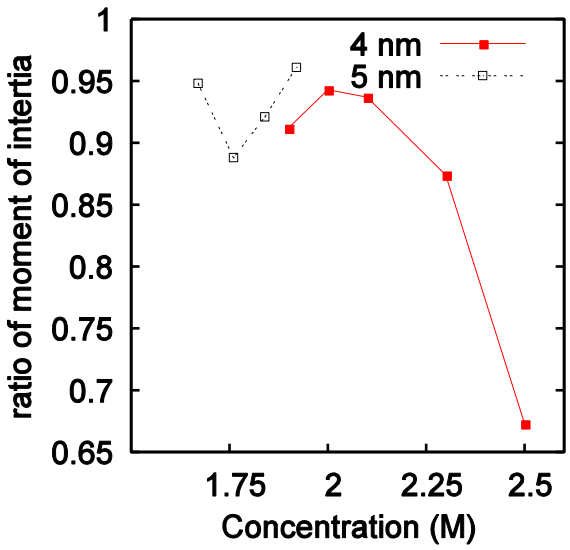

Figure 4.8: Variation of the ratio of moment of inertia, $\langle I_{xx}/I_{yy}\rangle/\langle I_{zz}/I_{yy}\rangle$, of the aggregate as a function of surfactant concentration, where I_{kk} denotes the moment of inertia around the k-axis through the center of mass of the aggregate. The labels are the gap sizes.

Table 4.3: Adsorption of octanoate molecules in sodium octanoate (SO) solutions confined between two parallel graphite walls.

Gap size (nm)	Number of SO molecules in simulation cell	Overall concentration (M)	Number of adsorbed molecules	Average of maximum aggregation number
3	60	2.0	55	
	72	2.5	69	
	86	3.0	59	
	100	3.5	64	
5	80	1.67	61	12
	84	1.76	63	16
	88	1.84	63	21
	92	1.92	66	20

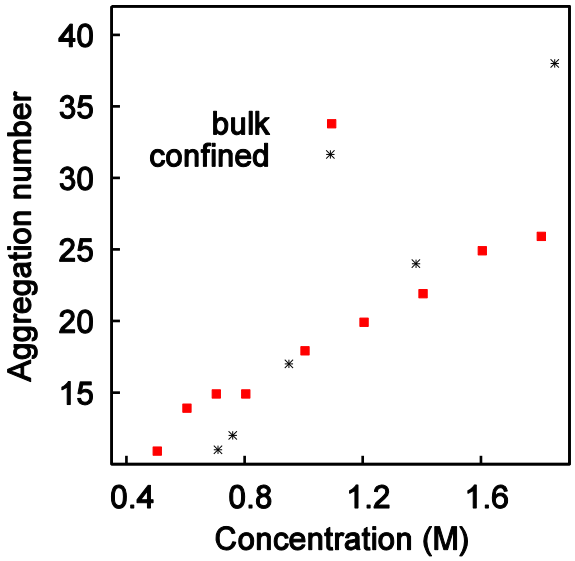

Figure 4.9: Variation of aggregation number with surfactant concentration for aggregates formed between two parallel graphite walls with a gap size of 4 nm ("confined") and in a bulk solution ("bulk"). The data for the bulk solution were taken from the experimental study by Zemb *et al*. (1983).

Table 4.2 also indicates that an aggregation number of 11 was first observed in a 4-nm gap at a surfactant concentration of 1.9 M. This concentration is in fact much higher than the normal critical micelle concentration (CMC) of SO in bulk solution, which is approximately 0.4 M (Kuhn, 1998). It is possible that this CMC shift is caused solely by the fact that a considerable amount of surfactants are adsorbed on the wall, hence reducing the number of "free" surfactants available for aggregation. Indeed, as shown in Table 4.2, with a gap size of 4 nm, an average of about 60 octanoate molecules are adsorbed on the walls. The variation of aggregation number with surfactant concentration is plotted in Figure 4.9 for two cases: a bulk SO solution and a SO solution confined between a 4-nm gap. The data for the bulk solution were taken from the experimental study by Zemb *et al*. (1983). For the confined case, the surfactant concentration was calculated based on the amount of "free" surfactants occupying a volume that is reduced by the thickness of the adsorbed layers, which was taken as 0.9 nm from each wall (see Figure 4.1). As shown in the figure, the aggregation number increases with increasing surfactant concentration in both cases. However, the rate of increase in the confined case is higher, and at high concentration (1.8 M) a large

aggregate appears in the confinement. This comparison, albeit qualitative, suggests that the CMC shift in a confined surfactant solution may be caused not only by surfactant adsorption, but also by other factors associated with the confining environment.

4.5 Effect of Gap Size on Adsorption

The numbers of adsorbed molecules in the 3-nm and 5-nm gaps are shown in Table 4.3 for different surfactant concentrations. In the 5-nm gap, adsorption is approximately constant for all the surfactant concentrations considered (1.67 M–1.92 M), a behaviour similar to that observed in the 4-nm gap. Rosen (2004) explained that the adsorption of SDS type of surfactant to hydrophobic adsorbents is of the Langmuir type, and Greenwood *et al.* (1968) reported that this type of adsorption would show surface saturation in the vicinity of the CMC. Similar adsorption behaviour was also reported by Muter *et al.* (2010). In the present simulation study of confined SO solutions, all the concentrations are above the CMC, and therefore it is reasonable to expect that surface saturation would occur in all three gap sizes.

The density profiles of the C8 atom and the oxygen atoms are plotted in Figure 4.10 for two cases: a 2.5 M SO solution confined in a 3-nm gap and a 1.9 M SO solution confined in a 4-nm gap. In both cases, 72 SO molecules are confined by two parallel graphite walls. In the 3-nm case, all the octanoate molecules are adsorbed, whereas in the 4-nm case, some octanoate molecules remain in the middle of the gap, as evidenced by the small peak in the C8 density profile at $z^* = 0$, where $z^* = z/(L/2)$, z is the distance from the mid plane, and L is the gap size. The difference in this behaviour may be understood by referring to the PMF between an octanoate anion and the graphite wall as shown in Figure 4.5. As shown in the figure, if an octanoate anion falls within about 1.4 nm from the wall, it is likely to be attracted to the wall as the potential minimum is located at $r \approx 0.4$ nm. However, if it is located beyond 1.4 nm, it may not feel the presence of the wall and may therefore tend to remain at the same location. In a 3-nm gap, the shape of the PMF between an octanoate anion and the graphite wall is likely to be similar to that shown in Figure 4.5, except that the width of the plateau

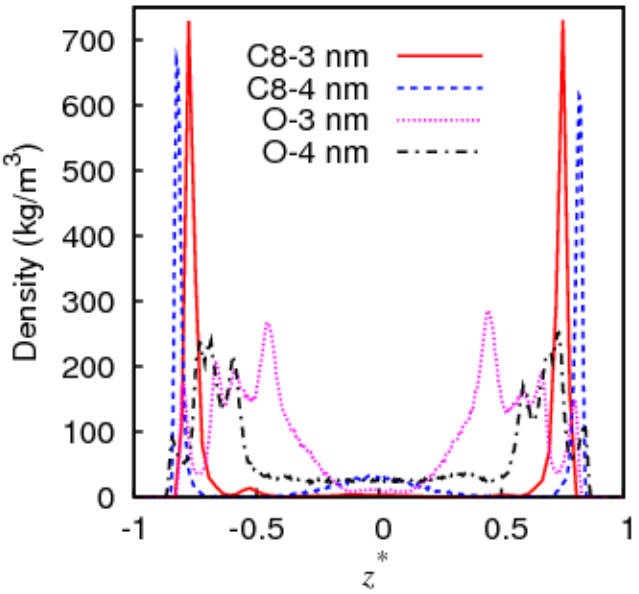

Figure 4.10: Density profiles of the last carbon atom (C8) and the oxygen atoms (O) of the octanoate molecule in a sodium octanoate (SO) solution confined by two parallel graphite walls with gap sizes of 3 nm and 4 nm. The SO solution contains 72 SO molecules. z^* is the distance from the mid-plane scaled by half of the gap size.

around the mid-plane may be reduced, mainly because the wall–octanoate interactions in this narrower gap will probably be stronger than those in the 4-nm gap. In a 3-nm gap, the mid-plane is only 1.5 nm away from the wall, which means that most octanoate molecules would likely migrate toward the wall surface; on the other hand, in a 4-nm gap, some octanoate molecules which are initially located near the mid-plane may not be attracted toward the wall, but self-assemble into aggregates instead.

4.6 Effect of Gap Size on Micelle Formation

As mentioned earlier, micelle formation was observed in the 4-nm and 5-nm gaps but not in the 3-nm gap. In addition to the difference in adsorption discussed in the preceding section, the observed difference may also be attributed to the fact that there is simply not sufficient space for micellization in a 3-nm gap. According to Hayter and Zemb (1982), the diameter of a small spherical SO micelle, with an aggregation number of 15, is about

2.3 nm in a bulk solution. Taking into account the thickness of the adsorbed surfactant layer in a 3-nm gap, there is only about 1.2 nm of "free" space within the gap (see Figure 4.10), making any surfactant micellization very difficult. In cases where very concentrated surfactant solutions (3.0 M and higher) are confined between a 3-nm gap (see Table 4.2), aggregate formation was observed, but these aggregates are neither spherical micelle nor bilayer, rather they form a single layer of parallel octanoate molecules.

Another aspect of confined micellization is related to the effects of external forces. As described by Israelachvilli (1992), the two major forces involved in the self-assembly of ionic amphiphilic molecules are hydrophobic forces and electrostatic interactions. If these forces are altered, by external interactions for example, then it is conceivable that the size or shape of the aggregate may be affected. To further study the possible effects of external forces on confined surfactant solutions, the PMF between a methane pair confined in a 4-nm gap was determined and is shown in Figure 4.11, together with a corresponding PMF obtained in a bulk solution. These PMFs should reflect the non-bonded interactions between two methylene groups, which, in turn, characterize the interactions of two hydrocarbon surfactant tails. The most distinctive difference between the two PMFs is the enhanced potential barriers at $r \approx 0.55$ nm and $r \approx 0.85$ nm in the PMF of the confined case. More specifically, in a SO solution confined between two graphite walls, the surfactant molecules may have to overcome larger repulsive potentials between the surfactant tails, compared to the bulk, before they can form an aggregate.

To discern the effects of confinement on the electrostatic interactions between the surfactant heads, the PMF between a pair of CH_3COO^- ions confined between two graphite walls and the corresponding PMF in a bulk solution are shown in Figure 4.12. Note that the potential in the confined case is generally lower than that in the bulk solution. This reduced electrostatic repulsion between the surfactant heads may facilitate the surfactant self-assembling process in the confined environment, thus counteracting the increased repulsive barriers between the surfactant tails discussed in the preceding paragraph. Consequently, the overall effect of the confinement on surfactant self-

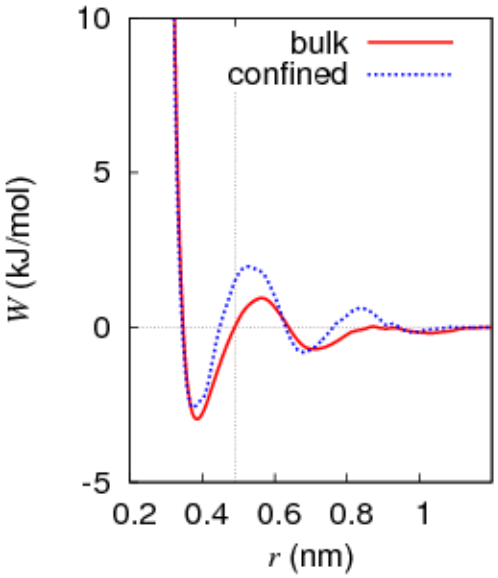

Figure 4.11: Potential of mean force between two methane molecules. The case in which two methane molecules are confined between two parallel graphite walls with a gap size of 4 nm is labeled as "confined", and the corresponding case in bulk water is labeled as "bulk".

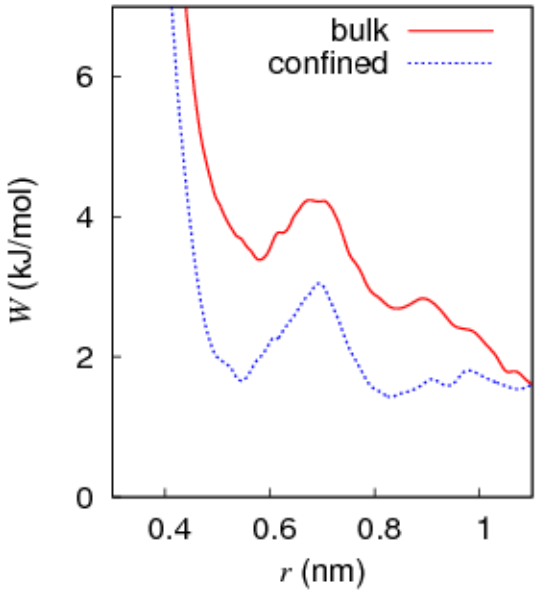

Figure 4.12: Potential of mean force between two CH_3COO^- ions. The case in which two sodium octanoate are confined between two parallel graphite walls with a gap size of 4 nm is labeled as "confined", and the corresponding case in bulk water is labeled as "bulk".

assembly will hinge on the balance between the altered van der Waals interactions and electrostatic interactions.

4.7 Water Structure in Confined SO Solutions

The formation of surfactant micelles in aqueous solutions is believed to be driven by the so-called hydrophobic effect (Tanford, 1980). More specifically, the water molecules surrounding a surfactant tail are relieved of their highly ordered structure as the surfactant molecules self-aggregate, thus lowering the free energy of the system. Consequently, in addition to the effects of confinement on the intermolecular forces as discussed in the preceding section, the water structure in a confined surfactant solution may also play an important role in determining the behaviour of confined surfactant self-assembly.

Consider a 2.0 M SO solution confined in a 3-nm gap. Figure 4.13 depicts the density distributions of the oxygen atoms (O) and the C8 atom of the octanoate molecule along the z direction. In this case, most octanoate molecules are adsorbed to the wall, with the head groups directed away from the wall. The probability distributions, $P(\theta_{OH})$, for the water molecules in different layers within the gap were calculated following the procedure described in Chapter 2 and are shown in Figure 4.14. The distance of the water layer from the mid-plane was varied to observe the water structure at different locations. At 0.5 nm and 1.0 nm from the mid-plane, the water molecules show strong structuring because of the presence of a layer of surfactant head groups (see Figure 4.13). More interestingly, however, at the mid-plane ($z = 0$), where the SO concentration is close to zero (see Figure 4.13), a weak structuring is still discernable, as the distribution $P(\theta_{OH})$ is not completely horizontal at this point. These probability distributions can be compared to those obtained for the case in which only water is confined by two graphite walls with a gap size of 4 nm. As shown in Figure 4.15, the water layer at $z = 1.5$ nm (i.e., 0.5 nm from the wall) shows some structuring, probably because of the effect of the wall. However, this structuring does not propagate beyond 1.0 nm from the wall. This comparison suggests that the water structure in a confined surfactant solution is different from that in confined pure water, mainly because the adsorbed surfactants help to align

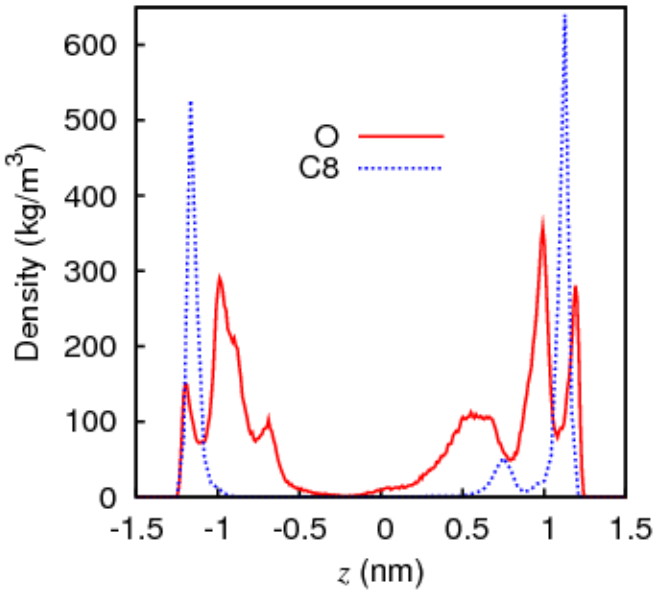

Figure 4.13: Density profiles of the oxygen atoms (O) and the C8 atom of the octanoate molecule in a 2.0 M sodium octanoate solution confined by two parallel graphite walls with a gap size of 3 nm. The distance z is the distance from the mid-plane along the z direction.

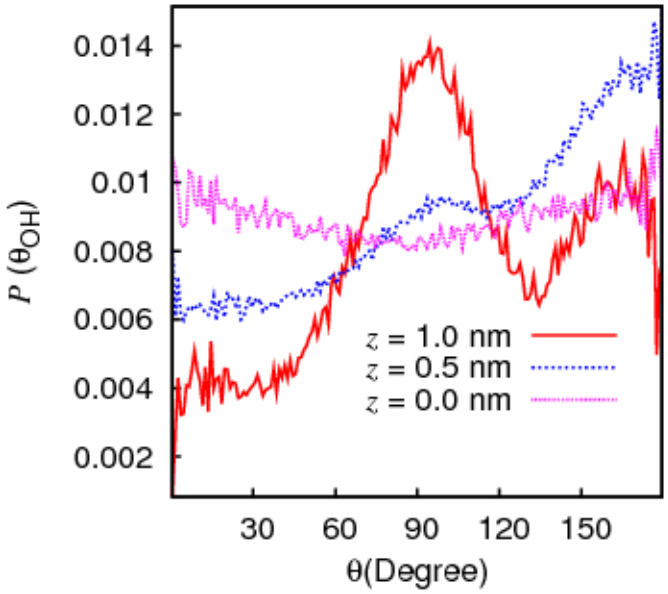

Figure 4.14: Probability distributions, $P(\theta_{OH})$, of the angle θ_{OH} between the water O–H bond and the inward normal to the wall. The water molecules are contained in different water layers, each 0.1 nm thick, at three locations (z = 0, 0.5, and 1.0 nm from the mid-plane). A 2.0 M sodium octanoate solution is confined by two parallel graphite walls with a gap size of 3 nm.

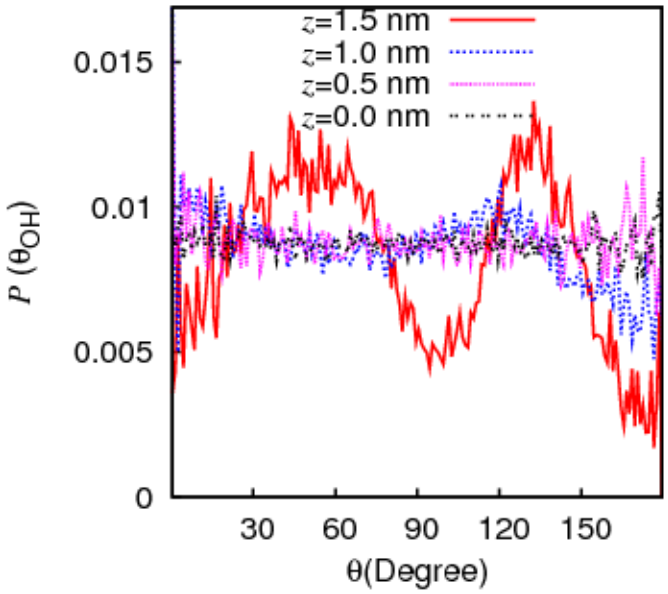

Figure 4.15: Probability distributions, $P(\theta_{OH})$, of the angle θ_{OH} between the water O–H bond and the inward normal to the wall. The water molecules are contained in different water layers, each 0.1 nm thick, at four locations (z = 0, 0.5, 1.0, and 1.5 nm from the mid-plane). Pure water is confined by two parallel graphite walls with a gap size of 4 nm.

water molecules even far away from the wall. Consequently, the micellization process between two parallel walls would, at least in principle, be different from that in a bulk solution.

4.8 Concluding Remarks

The results of this study have shown that the self-assembling behaviour of SO solutions confined between two parallel graphite walls, with gap sizes ranging from 3 to 5 nm, may be strongly affected by the confinement itself. The strong interactions between the octanoate tail and the graphite wall result in considerable surfactant adsorption, which plays a role in shifting the CMC of SO in confinement. More importantly, however, the presence of the confinement can alter the intermolecular interactions among the surfactant molecules, which in turn directly affects the self-assembling process, particularly the size and shape of the aggregates. In addition, the water molecules in a

confined surfactant solution can be aligned by the adsorbed surfactants, which further complicates the micellization process between two graphite walls.

CHAPTER 5

SODIUM OCTANOATE CONFINED BETWEEN TWO PARALLEL HYDROPHILIC AND HYDROPHOBIC SILICA WALLS

5.1 Introduction

This chapter examines the behaviour of SO solutions confined between two parallel hydrophilic silica walls and hydrophobic silica walls. In particular, the effects of surfactant concentration and gap size on surfactant self-assembly were studied using a series of constant-*NVT*, 120-ns MD simulations of confined SO solutions, with gap sizes of 3, 4, 5 and 6 nm. The simulation results reveal that, within the selected concentration ranges, SO forms bilayer structures between two silica walls. In the case of hydrophilic silica, with gap sizes of 3 nm and 4 nm, the bilayer structures are attached to the wall; however, when the gap size increases to 5 nm and 6 nm, the surfactant aggregates seem to form a bridge between two adsorbed layers of surfactants. In the case of hydrophobic silica wall, bilayer structures also appear, but the adsorbed SO molecules tend to adopt a different orientation from that observed with hydrophilic silica.

The remainder of this chapter is arranged as follows: the key aspects of hydrophilic silica confinement and its effects on the aggregate structure are discussed in sections 5.2 and 5.3. This is followed by a discussion of hydrophobic silica walls in section 5.4. Section 5.5 then presents a detailed analysis of the hydrophobic and electrostatic interactions involved in the two types of silica confinements. A short discussion on the water structure is given in section 5.6, and finally concluding remarks are given in section 5.7.

5.2 Bilayer Formation between Two Hydrophilic Silica Walls

The concentration ranges of the simulation cases related to hydrophilic silica wall are listed in Table 5.1. Note that these concentration ranges were selected with the objective

Table 5.1: Simulation cases considered in the study of hydrophilic silica confinement.

Numberof sodium octanoate molecules in simulation cell	Gap size (nm)	Overall surfactant concentration (M)
69	3	2.00
86	3	2.50
104	3	3.02
120	3	3.49
68	4	1.48
72	4	1.57
76	4	1.66
80	4	1.75
88	4	1.92
96	4	2.09
80	5	1.39
84	5	1.47
88	5	1.54
92	5	1.61
96	5	1.68
119	5	2.08
86	6	1.25
103	6	1.50
120	6	1.75
138	6	2.00

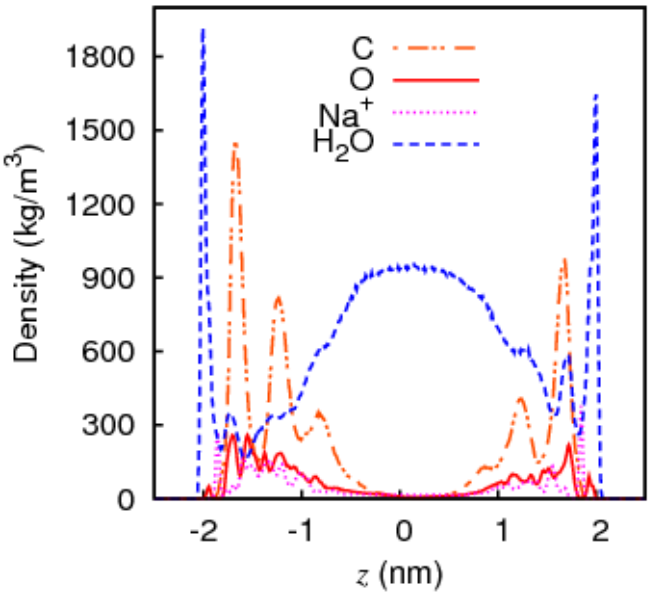

Figure 5.1: Time-averaged density distributions of various atomic groups along the *z*-axis in a 2.09 M sodium octanoate solution confined by two hydrophilic silica walls with a gap size of 4 nm. The distance *z* is the distance from the mid-plane of the two walls. The average was taken from the frames between 80 ns and 120 ns. C and O denote the methylene groups and the oxygen atoms of octanoate, respectively. Na^+ and H_2O carry their usual meaning.

of observing aggregate formation and the effects of gap size. The case in which a 2.09 M SO solution is confined between a 4-nm gap will be discussed first as a representative case. The density profiles of the oxygen atoms, methylene groups, counterion (Na^+), and water (H_2O) in the *z* direction, i.e., normal to the wall–solution interface, are shown in Figure 5.1. All these profiles suggest that no octanoate molecule is present in the middle region between the two walls. It is interesting to point out that the water density adjacent to the wall is very high; this dense water layer can also be observed in the snapshot shown in Figure 5.2, where the water molecules penetrate beyond the hydrogen layer of the walls. Surfactant molecules cluster along the walls, and from Figure 5.1, it appears that the surfactant tails form several layers, as there are several distinct peaks in the density profiles of the methylene groups. These layers of octanoate stay parallel to the walls, forming bilayers which can be visualized in Figure 5.3, where the density

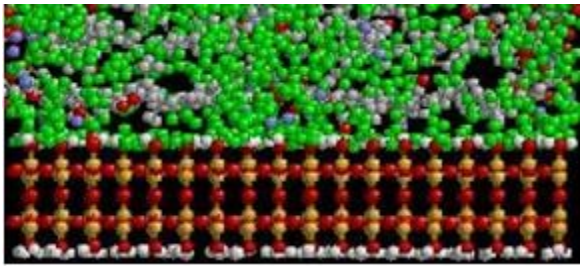

Figure 5.2: Snapshot (interfacial region) of sodium octanoate solution confined by two hydrophilic (hydroxylated) silica walls with a gap size of 4 nm and a concentration of 2.09 M (at 80 ns). Gray spheres represent the methylene groups of the octanoate molecule, red spheres represent oxygen atoms, blue spheres are Na^+ ion, yellow spheres represents silicon atoms, and white spheres represents hydrogen atoms. Water molecules are represented by green spheres.

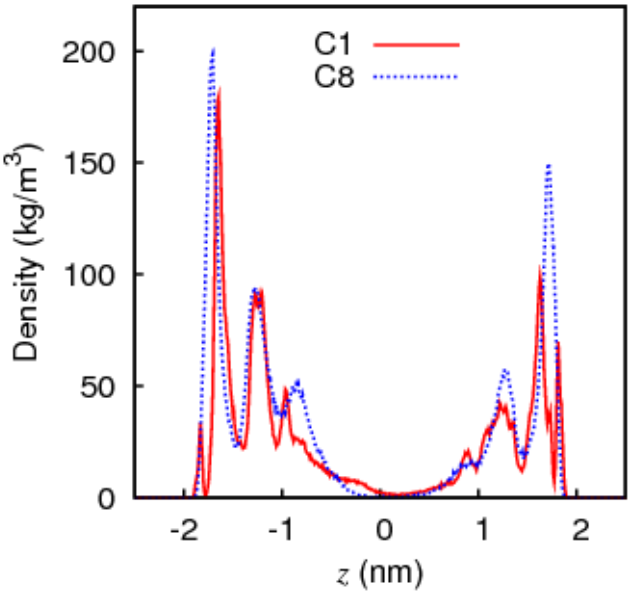

Figure 5.3: Time-averaged density distributions of the C1 and C8 atoms of the octanoate molecule along the *z*-axis in a 2.1 M sodium octanoate solution confined by two hydrophilic silica walls (gap size = 4 nm). The average was taken from the frames between 80 ns and 120 ns. C1 and C8 denote the first carbon atom and terminal methyl group, respectively, of the octanoate molecule from the head end. The distance *z* represents the distance from the mid-plane of the two walls.

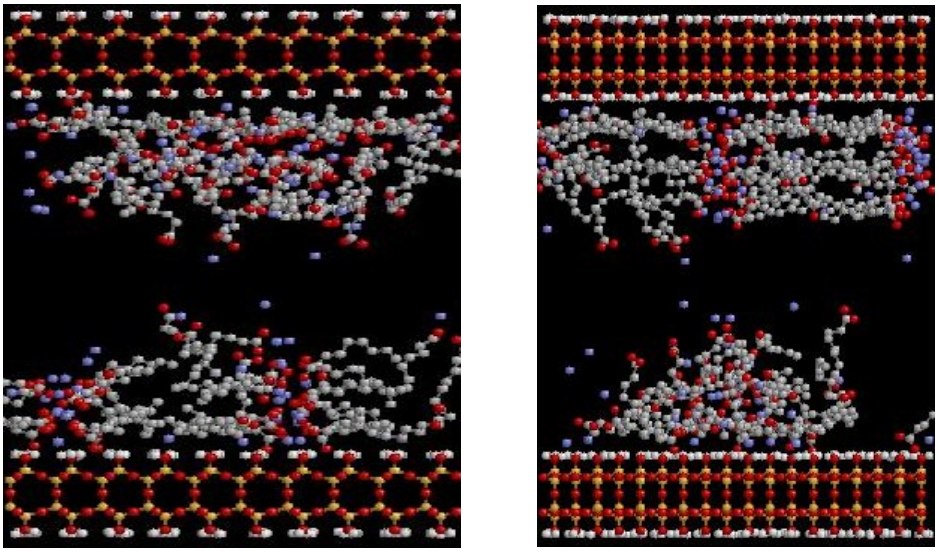

(a) (b)

Figure 5.4: Snapshots of a sodium octanoate solution confined by two hydrophilic silica (hydroxylated) walls with a gap size of 4 nm at a surfactant concentration of 2.09 M (at 80 ns). (a) *y*–*z* plane and (b) *x*–*z* plane. Gray spheres represent the methylene groups of an octanoate molecule, red spheres represent oxygen atoms, blue spheres are Na^+ ion, yellow spheres represent silicon atoms, and white spheres represent hydrogen atoms. Water molecules have been removed for clarity.

distributions of the C1 and C8 atoms are shown. Note that the peaks in the density profiles of C1 and C8 fall on each other. Figures 5.4a (*y*–*z* plane) and 5.4b (*x*–*z* plane) depict the snapshots of this case, showing the orientation of the octanoate molecules and the aggregates.

The observation that the bilayers are attached to the walls is consistent with the interactions between the hydrophilic silica wall and the various atomic groups of the octanoate anion. As shown in Figure 5.5, the PMF between the hydrophilic silica wall and a methane molecule displays a minimum in the vicinity of the wall. A similar trend is also observed for an acetate ion (CH_3COO^-) in Figure 5.6, where the PMF between the hydrophilic silica wall and an acetate ion has two minima in the vicinity of the wall as well. These two PMFs indicate that the octanoate anion prefers to move toward the wall.

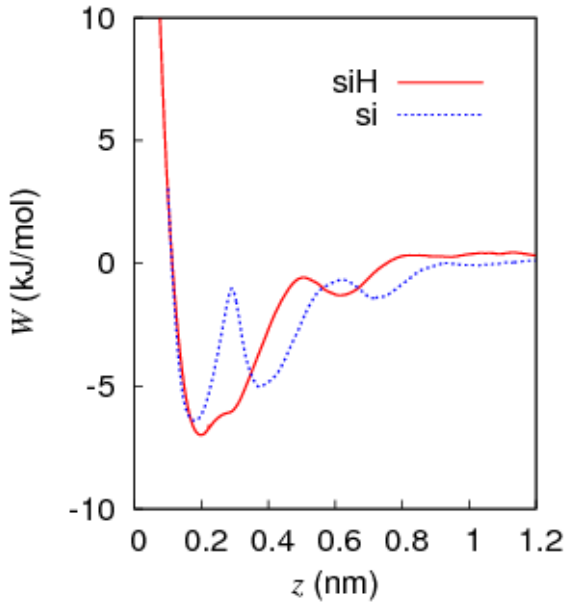

Figure 5.5: Potential of mean force between a methane (CH_4) molecule and the hydrophilic silica wall ("siH"), and between a CH_4 molecule and the hydrophobic silica wall ("si"). A CH_4 molecule is confined between two parallel silica walls with a gap size of 4 nm.

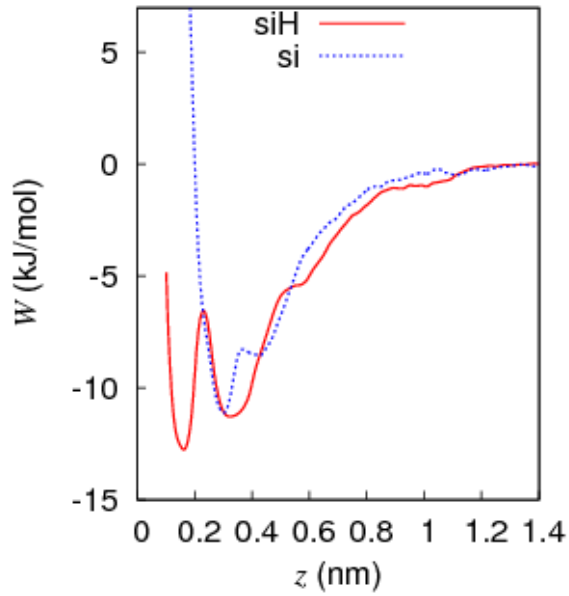

Figure 5.6: Potential of mean force between an acetate (CH_3COO^-) ion and a hydrophilic silica wall ("siH"), and between a CH_3COO^- ion and a hydrophobic silica wall ("si"). A CH_3COO^- ion and a Na+ ion are confined between two parallel silica walls with a gap size of 4 nm.

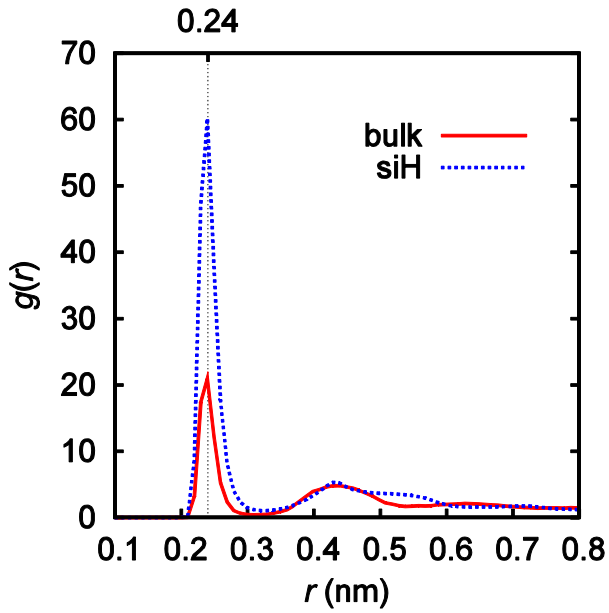

Figure 5.7: Radial distribution functions (RDFs) between a Na^+ ion and the oxygen atoms of an octanoate molecule in a 0.55 M sodium octanoate (SO) solution ("bulk") and in a 2.1 M SO solution confined by two parallel hydrophilic silica walls with a gap size of 4 nm ("siH"). The RDFs were calculated from the frames between 80 ns and 120 ns.

The bilayer structures observed in Figure 5.4 also indicate a strong pairing between the anionic head of octanoate and its counterion. Indeed, such a strong correlation can be assessed quantitatively by considering the radial distribution function (RDF) between the oxygen atoms of octanoate and Na^+, as shown in Figure 5.7. In this figure, the radial distribution function between the octanoate oxygen atoms and Na^+ in a confined 2.1 M SO solution is compared with that in a 0.55 M bulk SO solution, where spherical micelles are normally observed. Although the first peaks in both cases are located at the same distance (r = 0.24 nm), the $g(r)$ value in the confined case is much higher. The RDF of a pair of C1 atoms is also shown in Figure 5.8. Not only is the first peak in the confined case located at a shorter distance than that in the bulk case, its magnitude is also much larger, indicating that the octanoate surfactant heads are much more correlated in the confined case than in the bulk case.

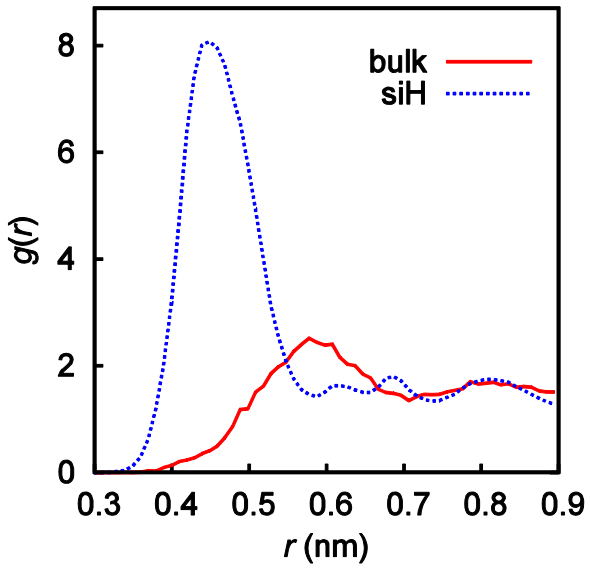

Figure 5.8: Radial distribution functions (RDFs) between two C1 atoms of the octanoate molecule in a 0.55 M sodium octanoate (SO) solution ("bulk") and in a 2.1 M SO solution confined by two parallel hydrophilic silica walls with a gap size of 4 nm ("siH"). The RDFs were calculated from the frames between 80 ns and 120 ns.

5.3 Effect of Surfactant Concentration and Gap Size in Hydrophilic Silica Cases

To study the effect of surfactant concentration on the self-assembling behaviour of confined SO solution, the gap size of 4 nm will be used as a base case. Bilayer formation was observed at all concentrations considered in this study (see Table 5.1), with a strong correlation between the oxygen atoms and the Na^+ ion at r = 0.24 nm as shown in Figure 5.9. The density profiles of the C8 and C1 atoms for three concentrations (1.48 M, 1.75 M, and 1.92 M) are shown in Figures 5.10a and 5.10b, respectively. As in the case of 2.1 M described above (see Figure 5.3), the fact that the peak locations in the C8 profiles coincide with those in the C1 profiles indicates that the octanoate molecules are almost parallel to the wall.

Similar bilayer structures and orientation of octanoate molecules were also observed in the case of 3-nm gap for all the surfactant concentrations considered (data not shown). However, as the gap size becomes larger than 4 nm, the octanoate molecules

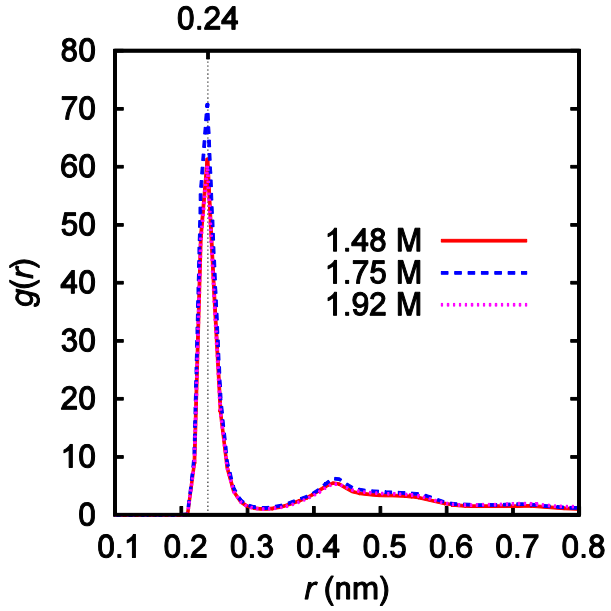

Figure 5.9: Radial distribution functions (RDFs) between a Na^+ ion and the oxygen atoms of an octanoate molecule at different concentrations. The sodium octanoate solution is confined between two parallel hydrophilic silica walls with a gap size of 4 nm. The RDFs were calculated from the frames between 80 ns and 120 ns.

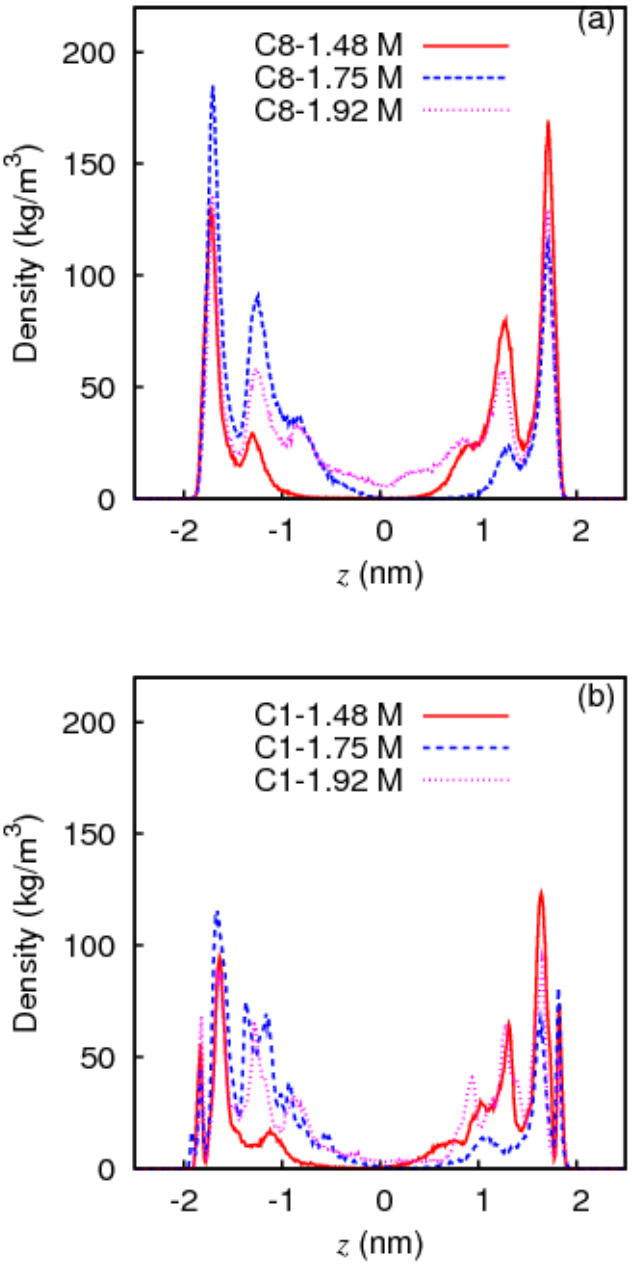

Figure 5.10: Time-averaged density distributions of the (a) C8 and (b) C1 atoms of octanoate along the *z*-axis in a sodium octanoate solution confined by two parallel hydrophilic silica walls with a gap size of 4 nm at different concentrations. C1 is attached to the two oxygen atoms and C8 is located at the tail end. The distance *z* represents the distance from the mid-plane of the two walls. The average is taken from the frames between 80 ns and 120 ns.

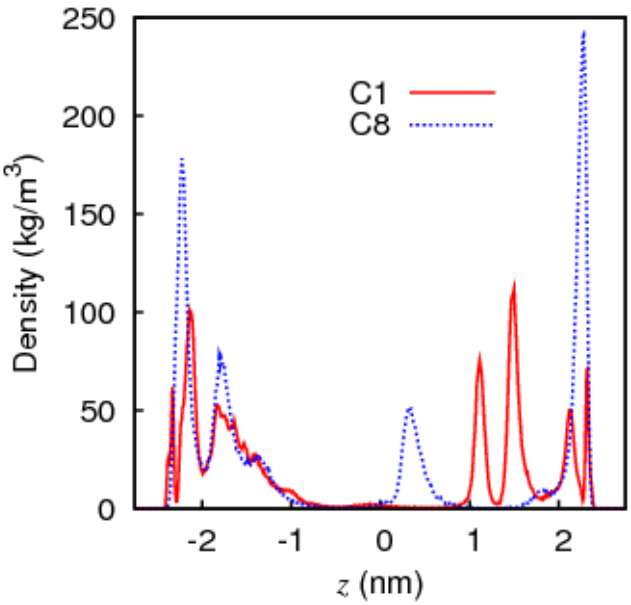

Figure 5.11: Time-averaged density distribution of the C8 and C1 atoms of octanoate along *z*-axis in a sodium octanoate solution confined by two parallel hydrophilic silica walls with a gap size of 5 nm and a surfactant concentration of 1.47 M. C1 is attached to the two oxygen atoms and C8 is located at the tail end. The distance *r* represents the distance from the mid-plane of the two walls. The average is taken from the frames between 80 ns and 120 ns.

adopt a different orientation while maintaining the bilayer structures. For example, Figure 5.11 depicts the density profiles of the C1 and C8 atoms of the octanoate molecule along the *z*-axis for a 1.47 M SO solution confined in a 5-nm gap. The peaks in both profiles at approximately –2.1 nm and –1.8 nm indicate two layers of octanoate molecules lying parallel to the wall. However, the distinct peaks in the C8 profile at about 0.3 nm and 2.2 nm, together with those in the C1 profile at about 1.1 nm and 1.5 nm, suggest that some octanoate molecules are oriented almost perpendicular to the wall. Indeed, the different orientations can be observed readily in Figure 5.12, which shows the snapshots of SO solutions at three different concentrations, 1.47 M, 1.54 M, and 1.68 M, confined in a 5-nm gap.

The behaviour of SO solutions confined in a 6-nm gap is similar to that observed in a 5-nm gap, i.e., bilayers of different orientations were observed depending on the

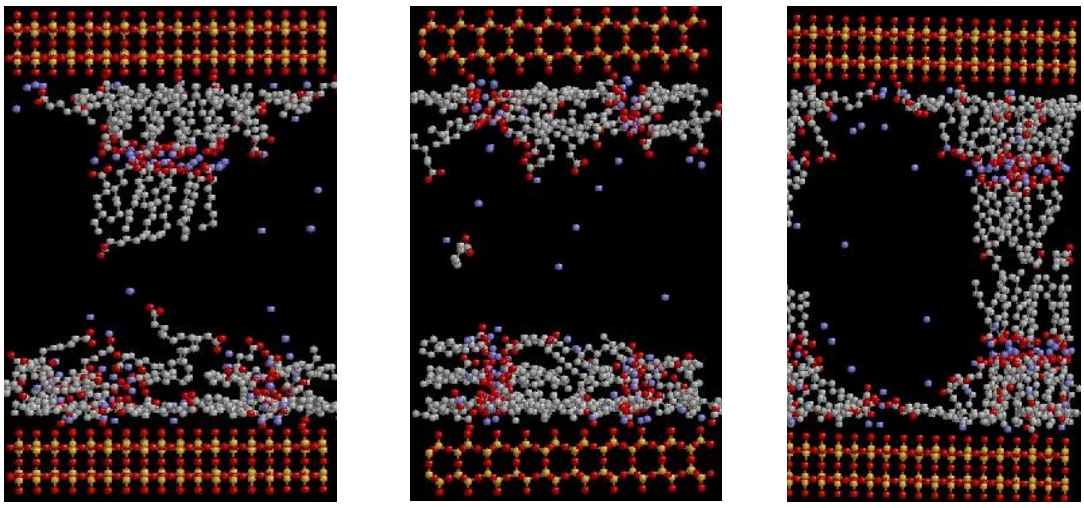

(a) (b) (c)

Figure 5.12: Snapshots of sodium octanoate solutions confined between two hydrophilic silica (hydroxylated) walls with a gap size of 5 nm at different concentrations (at 80 ns). (a) 1.47 M, (b) 1.54 M, (c) 1.68 M. Gray spheres represent the methylene groups of the octanoate molecule, red spheres represent oxygen atoms, blue spheres are Na^+ ion, and yellow spheres represents silicon atoms. Water molecules have been removed for clarity.

surfactant concentration. For example, at 1.25 M, the bilayers lie mostly parallel to the wall, whereas at 1.5 M, some perpendicular bilayers also appear (see Figure 5.13). It is worth noting that in some cases (see Figures 5.12a and 5.13b), the bilayers are attached in such a way that the hydrophobic tails of the octanoate molecules are exposed to water. This is in contrast to the general understanding of surfactant self-assembly in aqueous solution, where the hydrophobic tails are shielded from water to minimize the unfavorable interactions (the so-called hydrophobic effects) (Tanford, 1980). As discussed in Chapter 4, intermolecular interactions, particularly those between two surfactant molecules, may be altered by the confinement, which may lead to very different self-assembling behaviour. Section 5.5 will explore the possible effects of silica wall on the two main forces involved: hydrophobic interactions and electrostatic interactions.

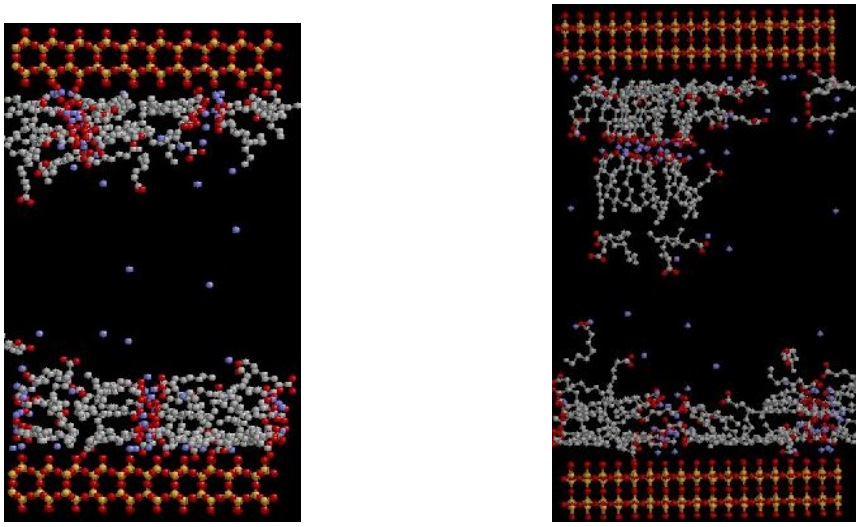

(a) (b)

Figure 5.13: Snapshots of sodium octanoate solutions confined by two hydrophilic silica (hydroxylated) walls with a gap size of 6 nm at different concentration (at 80 ns). (a) 1.25 M, (b) 1.50 M. Gray spheres represent the methylene groups of the octanoate molecule, red spheres represent oxygen atoms, blue spheres are Na^+ ion, and yellow spheres represents silicon atoms. Water molecules have been removed for clarity.

5.4 Bilayer Formation between Two Hydrophobic Silica Walls

Table 5.2 lists the concentration ranges used in the simulation study of hydrophobic silica wall. As in the case of the hydrophilic silica wall, we begin with a representative case where a 2.1 M SO solution is confined between a 4-nm gap. The density profiles of the oxygen atoms, methylene groups, counterion (Na+), and water (H_2O) in the *z* direction, i.e., normal to the wall–solution interface, is shown in Figure 5.14. Although the peak locations in the water profile and the methylene group profile seem to indicate that a layer of water is sandwiched between the surfactant tails and the wall, the snapshot shown in Figure 5.15 reveals that the water molecules are in fact in contact with the wall where it is not covered by the octanoate molecules.

Table 5.2: Simulation cases considered in the study of hydrophobic silica confinement.

Numberof sodium octanoate molecules in simulation cell	Gap size (nm)	Overall surfactant concentration (M)
69	3	2.00
86	3	2.50
104	3	3.00
120	3	3.50
68	4	1.50
72	4	1.60
76	4	1.70
80	4	1.80
96	4	2.10
80	5	1.39
84	5	1.47
88	5	1.54
92	5	1.61
96	5	1.68
119	5	2.08
52	6	0.75
69	6	1.00
86	6	1.25
103	6	1.50
120	6	1.75
138	6	2.00

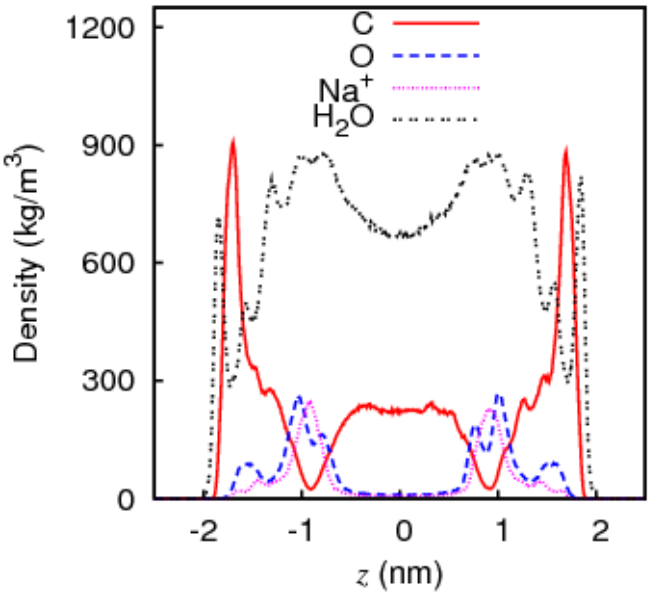

Figure 5.14: Time-averaged density distributions of various atomic groups along the *z*-axis in a 2.1 M sodium octanoate solution confined by two hydrophobic silica walls with a gap size of 4 nm. The distance *z* is the distance from the mid-plane of the two walls. The average was taken from the frames between 80 ns and 120 ns. C and O denote the methylene groups and the oxygen atoms of octanoate. respectively. Na^+ and H_2O carry their usual meaning.

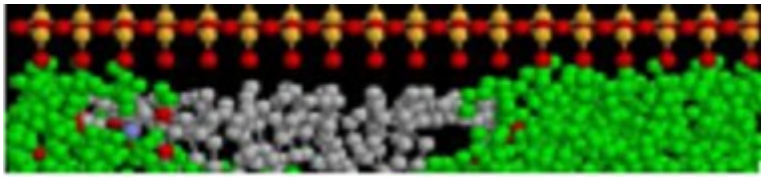

Figure 5.15: Partial snapshot showing the solid–liquid interface in a 2.1 M sodium octanoate solution confined by two hydrophobic silica walls with a gap size of 4 nm (at 80 ns). Gray spheres represent the methylene groups of the octanoate molecule, red spheres represent oxygen atoms, blue spheres are Na^+ ion, and yellow spheres represents silicon atoms. Water molecules are represented by green spheres.

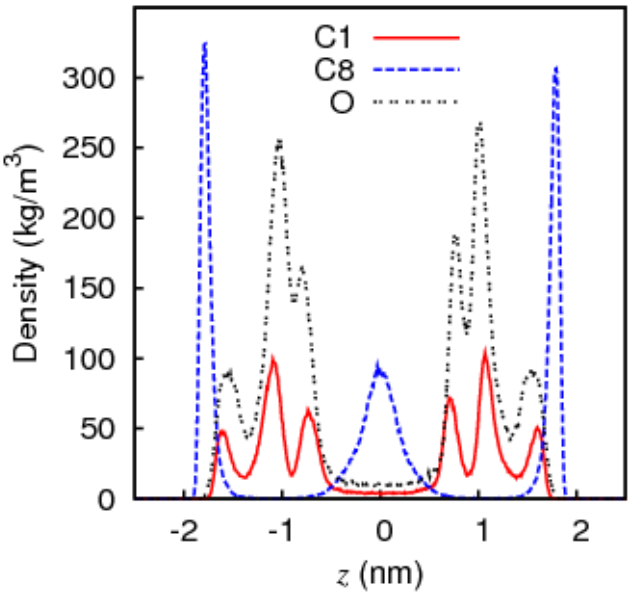

Figure 5.16: Time-averaged density distributions of the C1, C8, and oxygen atoms (O) of octanoate along the *z*-axis in a 2.1 M sodium octanoate solution confined by two hydrophobic silica walls with a gap size of 4 nm. The distance *z* is the distance from the mid-plane of the two walls. The average was taken from the frames between 80 ns and 120 ns. C1 and C8 represent the first carbon atom and the terminal methyl group, respectively, of octanoate from the head end.

Figure 5.16 depicts the density profiles of the C1, C8, and oxygen atoms of the octanoate molecule along the *z*-axis. The relative locations of the peaks of these profiles suggest that bilayer structures form between the two walls. In particular, as shown in the snapshots depicted in Figure 5.17, the middle region of the gap is filled with a bilayer structure, which is, in turn, confined by two adsorbed surfactant layers, with the tail ends of the octanoate molecules attached to the wall. This is in contrast to a similar case with hydrophilic silica walls (see Figure 5.4), where the octanoate molecules lie almost parallel to the wall. As discussed in section 5.3, with hydrophilic silica wall, the orientation of the adsorbed molecules may change, depending on the surfactant concentration and gap size. With hydrophobic silica wall, however, the adsorbed molecules are always perpendicular to the wall. It should also be noted that the orientation of the adsorbed octanoate molecules in hydrophobic silica confinement is

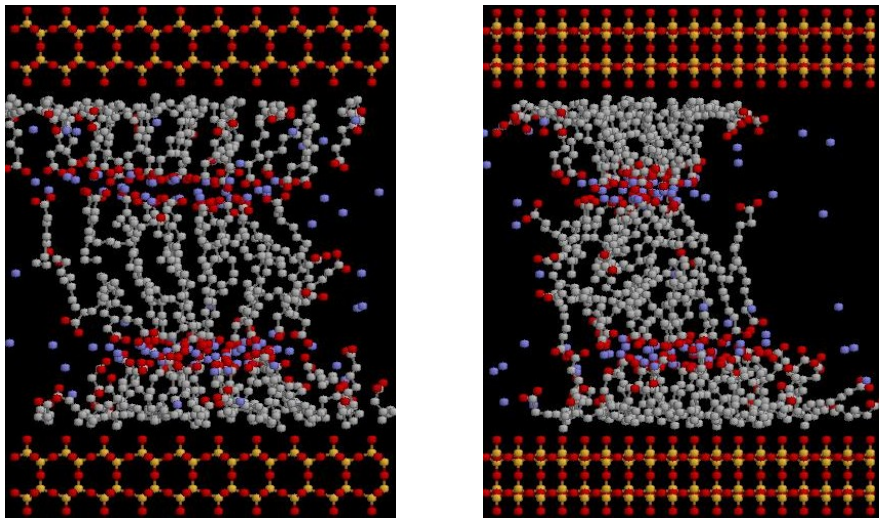

(a) (b)

Figure 5.17: Snapshots of a 2.1 M sodium octanoate solution confined by two hydrophobic silica walls with a gap size of 4 nm (at 80 ns). (a) *y–z* plane and (b) *x–z* plane. Gray spheres represent the methylene groups of an octanoate molecule, red spheres represent oxygen atoms, blue spheres are Na^+ ion, and yellow spheres represent silicon atoms. Water molecules have been removed for clarity.

similar to that in graphite confinement, except that in the graphite case spherical micelle was observed at higher concentrations.

The formation of bilayer structures between two adsorbed surfactant layers was also observed in other gap sizes. However, as the gap size increases, the number of layers of octanoate between the two walls also increases. For example, the 3-nm gap can accommodate three layers of octanoate, the 4- and 5-nm gaps can accommodate four layers, and the 6-nm gap can accommodate six layers (see Figure 5.18 for a snapshot). In all these cases, the octanoate layers are perpendicular to the wall.

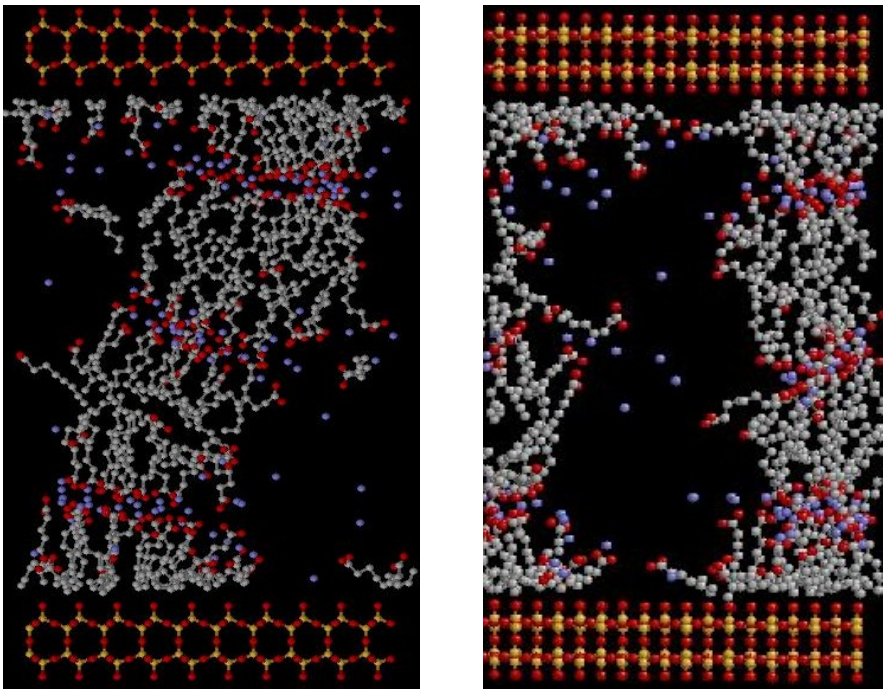

(a) (b)

Figure 5.18: Snapshot of a 1.75 M sodium octanoate solution confined between two hydrophobic silica walls with a gap size of 6 nm (at 80 ns). (a) *y*–*z* plane and (b) *x*–*z* plane. Gray spheres represent the methylene groups of an octanoate molecule, red spheres represent oxygen atoms, blue spheres are Na^+ ion, and yellow spheres represent silicon atoms. Water molecules have been removed for clarity.

5.5 Hydrophobic and Electrostatic Interactions in Silica Confinement

The interactions between two octanoate surfactant tails were assessed by calculating the PMFs of a methane–methane pair in water when confined in two parallel hydrophilic and hydrophobic silica walls with a gap size of 4 nm. These two PMFs are shown in Figure 5.19, together with the corresponding PMF obtained in a bulk solution. As shown in the figure, the interaction potential between two methane molecules within a 4-nm silica confinement is very similar to that in the bulk, which suggests that hydrophobic interactions are not affected by either of the two types of silica walls with a gap size of 4 nm.

To assess the electrostatic interactions between the octanoate head and Na^+, the PMF between a CH_3COO^- anion and Na^+ was calculated in a similar confinement and also in the bulk.

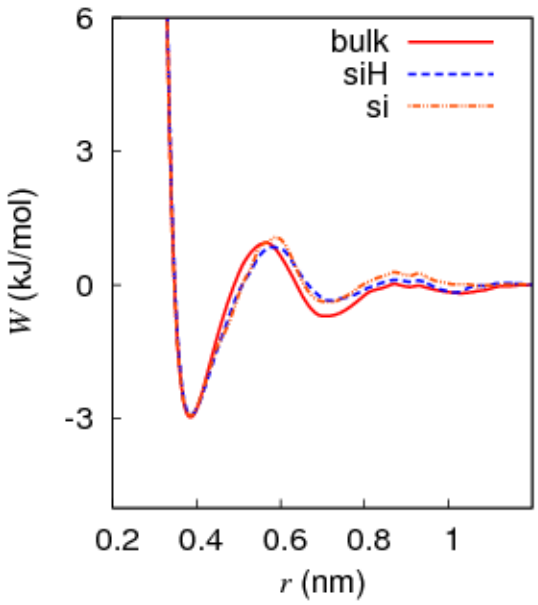

Figure 5.19: Potential of mean force between two methane molecules in water at infinite dilution ("bulk") and confined between two hydrophilic silica walls ("siH") and two hydrophobic silica walls ("si") with a gap size of 4 nm.

These two PMFs are shown in Figure 5.20. Note that in all three cases the first and second minima are located at approximately 0.27 nm (r_1) and 0.49 nm (r_2), respectively, and the first maxima are located at 0.38 nm (r_u). However, the values of $W(r_u)$, $W(r_1)$, and $W(r_2)$ in the confined cases are different from those in the bulk solution. More specifically, $W(r_1)$ in the confined cases is lower than that in the bulk solution, and the value of $\Delta W_{2u} = W(r_u) - W(r_2)$ in confined cases is also smaller than that in the bulk solution. Consequently, in a confined solution, it is comparatively easier for the two ions to approach each other and reach the potential minimum at 0.27 nm. In other words, the electrostatic interactions between a surfactant head and its counterion are altered by the confinement, resulting in the much stronger correlation shown in Figure 5.7. It is also noticed that this PMF is almost identical in hydrophobic and hydrophilic silica which

may indicate that the surface charge on hydrophilic silica wall is not affecting the interaction between head atoms of SO and counter ion.

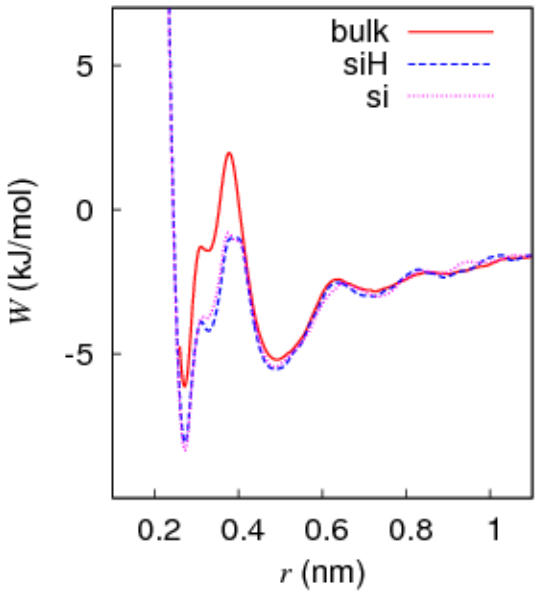

Figure 5.20: Potential of mean force between CH_3COO^- and Na^+ in water at infinite dilution ("bulk") and confined between two hydrophilic silica walls ("siH") and two hydrophobic silica walls ("si") with a gap size of 4 nm.

In addition to the interactions between a surfactant head and its counterion, the interactions between two surfactant heads also play a critical role in surfactant self-assembly. Figure 5.21 depicts the PMFs between two CH_3COO^- ions in two types of silica confinement and also in a bulk solution. Note that the potentials in the confined cases are generally lower than that in the bulk solution. In the bulk solution, the two anions may repel each other beyond 1 nm, but in both confined cases, they may stay at a closer distance, since the two minima in the PMFs are located at approximately 0.6 nm. Since the interactions between two acetate anions reflect those between two octanoate head groups, it is expected that in both silica cases, the head groups of the octanoate anions will experience a reduced repulsion. This reduced repulsion allows two surfactant

heads to come closer to each other, compared to a bulk solution (also see Figure 5.8), which would in turn facilitate the formation of bilayers.

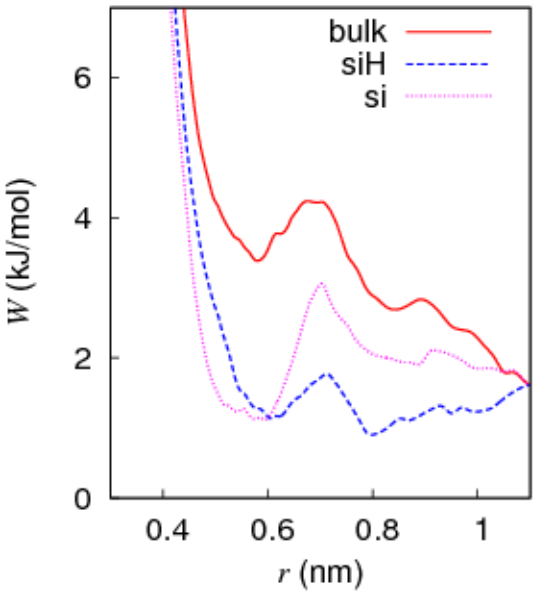

Figure 5.21: Potential of mean force between two CH_3COO^- ions in water at infinite dilution ("bulk") and confined between two hydrophilic silica walls ("siH") and two hydrophobic silica walls ("si") with a gap size of 4 nm.

5.6 Water Orientation and Bridge Structure

As discussed in section 4.7, surfactants adsorbed on a graphite wall are able to align the surrounding water molecules. A similar scenario was also observed in the cases of silica walls. More specifically, when the O atoms of the octanoate head groups form a layer in the confinement, the surrounding water molecules are aligned to a specific orientation. Consequently, the system's tendency to gain entropy by releasing the ordered structure of water molecules around the surfactant tails through micellization may, to some extent, be impeded by the adsorbed surfactants. Thus, in addition to the strong electrostatic attractions between the surfactant head and its counterion, as discussed in the preceding section, the formation of the bilayer structure observed in silica confinement, where two

layers of O atoms come in close contact, may also reduce the number of water molecules in the vicinity of the surfactant heads and help to increase the system entropy.

5.7 Concluding Remarks

The simulation results indicate that, within the gap-size and concentration ranges considered in this study, bilayer formation in SO solutions is induced by the presence of either hydrophilic or hydrophobic silica confinement. In the case of hydrophilic silica wall, the orientation of the bilayer structures changes as the gap size increases from 3 or 4 nm to 5 nm or higher. On the other hand, with hydrophobic silica wall, the adsorbed octanoate molecules are always perpendicular to the wall, and the number of octanoate layers filling the gap depends on the gap size. The formation of bilayer structures in both hydrophilic and hydrophobic silica confinements is likely a result of the enhanced electrostatic attractions between the anionic octanoate head group and their counterions, as well as the reduced repulsion between two octanoate head groups.

CHAPTER 6

CONCLUSION AND FUTURE WORK

This study was motivated by the need for an in-depth understanding of surfactant self-assembly in confined geometries. A series of *NVT* MD simulation was completed to explore the effects of confinement characteristics, gap size, and surfactant concentration on the self-assembling behaviour of confined SO solutions. All three factors were found to have considerable effects on the morphology of confined micelles. More specifically, in graphite confinement, the octanoate molecules tend to adsorb on the graphite walls at lower concentrations, but they start to form micellar aggregates at higher concentrations, when the walls are densely covered with surfactants. Spherical micelles form in the 4-nm and 5-nm gaps but not in the 3-nm gap. In addition, as the surfactant concentration increases, the shape of the micelle also changes. As revealed by the PMF, the strong interactions between the octanoate tail and the wall result in considerable surfactant adsorption, which plays a key role in shifting the CMC of SO in confinement. Moreover, water molecules adopt an ordered structure as the surfactant molecules form layers in the confinement, which may also affect the micellization process.

Surfactant bilayers were observed in both hydrophilic and hydrophobic silica confinements. With hydrophilic silica and smaller gap sizes (3 nm and 4 nm), these bilayers are parallel to the wall; however, when the gap size increases to 5 nm and 6 nm, the aggregates seem to form a bridging structure between two adsorbed layers of surfactants. In contrast, the adsorbed SO molecules remain perpendicular to the hydrophobic silica wall in all cases, often forming bridges across the gap. As noted in Chapter 1, drilling with water-based drilling fluids may benefit from the blockage of shale pores in the near-wellbore region, since it may minimize water penetration into shale. The results of this study indicate that formation of such blocking structures is indeed possible under certain conditions, and, in principle, the bridging structures

observed in both types of silica confinement may help to reduce fluid flow through a tight porous medium.

Perhaps the most important finding of this study is that intermolecular interactions between surfactant molecules can be altered by the presence of the confining boundaries. Indeed, the formation of bilayers in silica confinement, as opposed to spherical micelles in graphite confinement, can be attributed to the enhanced electrostatic interactions between the charged surfactant head groups. In addition, a comparison of the PMFs in confined and bulk solutions indicates that hydrophobic interactions between surfactant molecules are also affected by the confining boundaries. As stated in section 1.3, surfactant micellization is a direct result of different intermolecular interactions in the surfactant solution. Thus, it is reasonable to conclude that the confining boundaries have a direct influence on the surfactant self-assembling process in confined geometries. Although previous studies have shown that CMC shift is caused by wall–surfactant interactions and the finite size effect of the gap (Zhang *et al.*, 2007), the results of this simulation study strongly suggest that a confining boundary can change the behaviour of a surfactant solution by directly affecting the interactions among the surfactant molecules themselves.

6.1 Future Work

The results of this simulation study have revealed some interesting behaviour of confined surfactant solutions, particularly the effects of confinement on the morphology of surfactant aggregates and the interactions among surfactant molecules. However, the configuration space explored in this study is somewhat limited, as only small ranges of gap sizes, confinement characteristics, and surfactant concentrations have been considered. To enhance the fundamental understanding of these important systems and to exploit their unique properties for practical applications, further research along the line of this study is required. The following outlines some future research possibilities, which should contribute to the fundamental knowledge of surfactant self-assembly in confined geometries:

(i) The simulation results presented here suggest that similar studies should be extended to include other confinement geometries, such as rectangular tubes, cylindrical tubes, or spherical confinement. These confinement geometries may reveal additional interesting behaviour of confined surfactant solutions, especially the micellar morphology. In addition, as noted in Chapter 1, many nanomaterials have been synthesized using micelles as templates (Lisiecki *et al.*, 1996; Pileni, 1997); thus, the outcomes of this research may also be helpful in developing novel techniques for manufacturing nanomaterials.

(ii) The case of ionic surfactants in a *charged* confinement should also be investigated in more details, since electrostatic interactions would have a dominant effect in these cases. A wall with net Coulombic charges may alter the orientation of the adsorbed molecules, which would affect the morphology of the adsorbed aggregates. Moreover, electrostatic interactions in ionic surfactant solutions are likely to be greatly affected by the charged walls, particularly when the gap sizes are very small.

(iii) Canonical Monte Carlo simulations of confined surfactant solutions have revealed some peculiar features (Yuet, 2004), and the results of this study may have opened a path to further investigate the behaviour of these systems at the molecular level. Extended simulations (μs–ms range) of a relatively large system (on the order of 30,000 water molecules) are required to observe surfactant self-assembly and any secondary micelle structuring in confined surfactant solutions, which are currently not practical due to the high computational demand. An alternative is to use the Langevin dynamics (LD) technique, in which the effects of the solvent molecules are treated as the frictional and random forces. This implicit treatment of solvent molecules would make a large-scale simulation feasible with the existing computational facility. The LD technique has been used to simulate solutions containing surfactants with a large number of methylene sites and a low CMC (Shinto *et al.*, 2005; Shinto *et al.*, 2010). The effective interactions between the solutes are represented by the PMFs between the constituent site pairs. In the case of

SDS, for example, the site pairs can be identified as: (i) methane–sulfate, (ii) methane–methane, (iii) sulfate–sulfate, (iv) sodium (Na^+)–sulfate, (v) Na^+–methane, (vi) Na^+– Na^+, (vii) methane–wall, (viii) sulfate–wall, and (ix) Na^+–wall. Note that great care is required to validate the LD technique for use in studying surfactant self-assembly in confined geometries, and the results of the present study may be used for validation purposes.

(iv) In porous media, surfactant self-assembly may occur in a flowing system. Since CMC is also lowered by shear flow (Jones *et al.*, 1995), the combination of confinement and flow may provide useful and interesting insight into confined surfactant solutions. Many researchers have successfully used non-equilibrium MD simulations to investigate fluid flow through nanochannels (Yang, 2006; Zhu *et al.*, 2005; Wang *et al.*, 2011). In this case, an external driving force can be applied in the direction of flow to force the surfactant solution to flow through a channel. To set up such a simulation, velocities in all directions except that in the direction of flow will be thermostated; in the direction of flow, however, the thermostated velocity is that relative to the streaming velocity (Zhu *et al.*, 2005).

References

Allen, M. P.; Tildesley, D. J. *Computer Simulation of Liquids*; Oxford Science: New York, 1987.

Anilkumar, P.; Jayakannan, M. Single-molecular-system-based selective micellar templates for polyaniline nanomaterials: Control of shape, size, solid state ordering, and expanded chain to coillike conformation. *Macromolecules* **2007***, 40*, 7311−7319.

Atkin, R.; Craig, V. S. J.; Wanless, E. J.; Biggs, S. Mechanism of cationic surfactant adsorption at the solid-aqueous interface. *Adv. Colloid Interface Sci.* **2003***, 103*, 219−304.

Bandyopadhyay, S.; Shelley, J.; Tarek, M.; Moore, P.; Klein, M. Surfactant aggregation at a hydrophobic surface. *J. Phys. Chem. B* **1998***, 102*, 6318−6322.

Berendsen, H. J. C. GROMACS: a message-passing parallel molecular dynamics implementation. *Comput. Phys. Commun.* **1995***, 91*, 43−56.

Berendsen, H. J. C.; Postma, J. P. M.; van Gunsteren, W. F.; DiNola, A.; Haak, J. R. Molecular dynamics with coupling to an external bath. *J. Chem. Phys.* **1984***, 81*, 3684−3690.

Berendsen, H. J. C.; Postma, J. P. M.; van Gunsteren, W. F.; Hermans, J. Interaction models for water in relation to protein hydration. *Intermolecular Forces* **1981**, 331−342.

Blankschtein, D.; Thurston, G. M.; Benedek, G. B. Phenomenological theory of equilibrium thermodynamic properties and phase separation of micellar solutions. *J. Chem. Phys.* **1986***, 85*, 7268−7288.

Bowen, W. R.; Sharif, A. O. Long-range electrostatic attraction between like-charge spheres in a charged pore. *Nature* **1998***, 393*, 663−665.

Bruce, C. D.; Senapati, S.; Berkowitz, M. L.; Perera, L.; Forbes, M. D. E. Molecular dynamics simulations of sodium dodecyl sulfate micelle in water: the behavior of water. *J. Phys. Chem. B* **2002a***, 106*, 10902−10907.

Bruce, C. D.; Berkowitz, M. L.; Perera, L.; Forbes, M. D. E. Molecular dynamics simulation of sodium dodecyl sulfate micelle in water: Micellar structural characteristics and counterion distribution. *J. Phys. Chem. B* **2002b***, 106*, 3788−3793.

Carbajal-Tinoco, M. D.; Castro-Roman, F.; Arauz-Lara, J. L. Static properties of confined colloidal suspensions. *Phys. Rev. E: Stat. , Nonlinear, Soft Matter Phys.* **1996***, 53*, 3745−3749.

Cheong, D. W.; Panagiotopoulos, A. Z. Monte Carlo simulations of micellization in model ionic surfactants: Application to sodium dodecyl sulfate. *Langmuir* **2006***, 22*, 4076−4083.

Choudhury, N.; Ghosh, S. K. Colloidal suspensions in charged cylindrical pores: A perturbative density functional approach. *J. Chem. Phys.* **1999***, 111*, 1737−1745.

Choudhury, N.; Pettitt, B. M. Dynamics of water trapped between hydrophobic solutes. *J. Phys. Chem. B* **2005***, 109*, 6422−9.

Ciccotti, G.; Ferrario, M.; Hynes, J. T.; Kapral, R. Constrained molecular dynamics and the mean potential for an ion pair in a polar solvent. *Chem. Phys.* **1989***, 129*, 241-51.

Cracknell, R. F.; Gubbins, K. E.; Maddox, M.; Nicholson, D. Modeling Fluid Behavior in Well-Characterized Porous Materials. *Acc. Chem. Res.* **1995***, 28*, 281−288.

Crocker, J. C.; Grier, D. G. Methods of Digital Video Microscopy for Colloidal Studies. *J. Colloid Interface Sci.* **1996a***, 179*, 298−310.

Crocker, J. C.; Grier, D. G. When like charges attract: The effects of geometrical confinement on long-range colloidal interactions. *Phys. Rev. Lett.* **1996b***, 77*, 1897−1900.

D'Alessandro, M.; Tenenbaum, A.; Amadei, A. Dynamical and statistical mechanical characterization of temperature coupling algorithms. *J. Phys. Chem. B* **2002***, 106*, 5050−5057.

Davis, J. R.; Panagiotopoulos, A. Z. Micellization and phase separation in binary amphiphile mixtures. *Mol. Phys.* **2009***, 107*, 2359−2366.

de Moura, A. F.; Freitas, L. C. G. Molecular dynamics simulation of the sodium octanoate micelle in aqueous solution. *Chem. Phys. Lett.* **2005***, 411*, 474−478.

Dominguez, H.; Goicochea, A.; Mendoza, N.; Alejandre, J. Computer simulations of surfactant monolayers at solid walls. *J. Colloid Interface Sci.* **2006***, 297*, 370−373.

Dominguez, H. Self-aggregation of the SDS surfactant at a solid-liquid interface. *J. Phys. Chem. B* **2007***, 111*, 4054−4059.

Ducker, W.; Grant, L. Effect of substrate hydrophobicity on surfactant surface-aggregate geometry. *J. Phys. Chem.* **1996***, 100*, 11507−11511.

Eriksson, F.; Eriksson, J. C.; Stenius, P. Thermodynamics of micelle formation: model calculations for alkyl carboxylates. *Colloids Surf.* **1981***, 3*, 339–356.

Esselink, F. J.; Semenov, A. N.; ten Brinke, G.; Hadziioannou, G.; Oostergetel, G. T. Ordering of block copolymer micelles in confined two-dimensional solutions. *Macromolecules* **1995***, 28*, 3479–3481.

Floriano, M. A.; Caponetti, E.; Panagiotopoulos, A. Z. Micellization in model surfactant systems. *Langmuir* **1999***, 15*, 3143–3151.

Gandhi, N. S.; Mancera, R. L. Can current force fields reproduce ring puckering in 2-O-sulfo-alpha-L-iduronic acid? A molecular dynamics simulation study. *Carbohydr. Res.* **2010***, 345*, 689–95.

Gao, J.; Ge, W.; Hu, G.; Li, J. From Homogeneous Dispersion to MicellesA Molecular Dynamics Simulation on the Compromise of the Hydrophilic and Hydrophobic Effects of Sodium Dodecyl Sulfate in Aqueous Solution. *Langmuir* **2005***, 21*, 5223–5229.

Gersappe, D. Modelling micelle formation in confined geometries . *High Perform. Polymers* **2000***, 12*, 573–579.

Giovambattista, N.; Debenedetti, P. G.; Rossky, P. J. Effect of Surface Polarity on Water Contact Angle and Interfacial Hydration Structure. *J. Phys. Chem. B* **2007***, 111*, 9581–9587.

Giovambattista, N.; Rossky, P. J.; Debenedetti, P. G. Effect of temperature on the structure and phase behavior of water confined by hydrophobic, hydrophilic, and heterogeneous surfaces. *J. Phys. Chem. B* **2009***, 113*, 13723–13734.

Giovambattista, N.; Rossky, P. J.; Debenedetti, P. G. Effect of pressure on the phase behavior and structure of water confined between nanoscale hydrophobic and hydrophilic plates. *Phys. Rev. E: Stat. , Nonlinear, Soft Matter Phys.* **2006***, 73*, 041604/1–041604/14.

GNU. GNU - GSL Scientific Library. *http://www.gnu.org/s/gsl/* (accessed 08/31, 2010).

Goloub, T. P.; Koopal, L. K.; Bijsterbosch, B. H.; Sidorova, M. P. Adsorption of Cationic Surfactants on Silica. Surface Charge Effects. *Langmuir* **1996***, 12*, 3188–3194.

Gonzalez-Perez, A.; Prieto, G.; Ruso, J.; Sarmiento, F. Thermodynamics of self-assembly of sodium octanoate: comparison with a fully fluorinated counterpart. *Mol. Phys.* **2003***, 101*, 3185–3195.

Goulding, D.; Hansen, J. P. Effective interaction between charged colloidal particles near a surface. *Mol. Phys.* **1998***, 95*, 649–655.

Grant, L.; Ederth, T.; Tiberg, F. Influence of surface hydrophobicity on the layer properties of adsorbed nonionic surfactants. *Langmuir* **2000***, 16*, 2285−2291.

Greenwood, F. G.; Parfitt, G. D.; Picton, N. H.; Wharton, D. G. *Adsorption from aqueous solution;* Adv. Chem. Series; American Chemical Society: Washington, DC, 1968; Vol. 79, pp 135−144.

Grier, D. G. Optical tweezers in colloid and interface science. *Curr. Opin. Colloid Interface Sci.* **1997***, 2*, 264−270.

Hayter, J.; Zemb, T.
Concentration-dependent structure of sodium octanoate micelles. *Chem. Phys. Lett.* **1982***, 93*, 91−94.

Henderson, D. In *Fundamentals of Inhomogeneous Fluids.* Henderson, D., Ed.; Marcel Dekker, Inc: New York, 1992.

Hess, B.; Kutzner, C.; van, d. S.; Lindahl, E. GROMACS 4: Algorithms for Highly Efficient, Load-Balanced, and Scalable Molecular Simulation. *J. Chem. Theory Comput.* **2008***, 4*, 435−447.

Hines, J. Theoretical aspects of micellisation in surfactant mixtures. *Curr. Opin. Colloid Interface Sci.* **2001***, 6*, 350−356.

Hirunsit, P.; Balbuena, P. B. Effects of confinement on water structure and dynamics: a molecular simulation study. *J. Phys. Chem. C* **2007***, 111*, 1709−1715.

Holmberg, K.; Andersson, M.; Palmqvist, A. Use of Self-Assembled Surfactants for Nanomaterials Synthesis*;* In *Particulate Systems in Nano- and Biotechnologies*; Ei-Shall, H., Ed.; CRC Press, 2008; pp 27−51.

Hu, Z.; Jiang, J. Assessment of biomolecular force fields for molecular dynamics simulations in a protein crystal. *J. Comput. Chem.* **2010***, 31*, 371−380.

Iler, R. K. *The Chemistry of Silica: Solubility, Polymerization, Colloid and Surface Properties, and Biochemistry*; Wiley: New Jersey, 1979.

Ise, N.; Okubo, T.; Sugimura, M.; Ito, K.; Nolte, H. J. Ordered Structure in Dilute-Solutions of Highly Charged Polymer Lattices as Studied by Microscopy .1. Interparticle Distance as a Function of Latex Concentration. *J. Chem. Phys.* **1983***, 78*, 536−540.

Israelachvili, J. *Intermolecular and surface forces*; Academic Press: New York, 1992.

Israelachvili, J. N.; Mitchell, D. J.; Ninham, B. W. Theory of Self-Assembly of Lipid Bilayers and Vesicles. *Biochim. Biophys. Acta* **1977***, 470*, 185−201.

Israelachvili, J. N.; Mitchell, D. J.; Ninham, B. W. Theory of Self-Assembly of Hydrocarbon Amphiphiles into Micelles and Bilayers. *J. Chem. Soc. , Faraday Trans. 2* **1976***, 72*, 1525–1568.

Jones, J. L.; Marques, C. M.; Joanny, J. -F. Shear-induced micellization of diblock copolymers. *Macromolecules* **1995***, 28*, 136–142.

Jorge, M. Molecular dynamics simulation of self-assembly of n-decyltrimethylammonium bromide micelles. *Langmuir* **2008***, 24*, 5714–5725.

Ju, S.; Chang, J.; Lin, J.; Lin, Y. The effects of confinement on the behavior of water molecules between parallel Au plates of (001) planes. *J. Chem. Phys.* **2005***, 122*, 1–5.

Katsube, T. J.; Nudford, B. S.; Best, M. E. Petrophysical characteristics of shales from the Scotian shelf. *Geophysics* **1991***, 56*, 1681–1689.

Kepler, G. M.; Fraden, S. Attractive potential between confined colloids at low ionic strength. *Phys. Rev. Lett.* **1994***, 73*, 356–359.

Ketner, A. M.; Kumar, R.; Davies, T. S.; Elder, P. W.; Raghavan, S. R. A simple class of photorheological fluids: Surfactant solutions with viscosity tunable by light. *J. Am. Chem. Soc.* **2007***, 129*, 1553–1559.

Kuhn, H.; Breitzke, B.; Rehage, H. The phenomenon of water penetration into sodium octanoate micelles studied by molecular dynamics computer simulation. *Colloid Polym. Sci.* **1998***, 276*, 824–832.

Larsen, A. E.; Grier, D. G. Like-charge attractions in metastable colloidal crystallites. *Nature* **1997***, 385*, 230–233.

Layfield, J. P.; Troya, D. Molecular Simulations of the Structure and Dynamics of Water Confined between Alkanethiol Self-Assembled Monolayer Plates. *J. Phys. Chem. B* **2011***, 115*, 4662–4670.

Lazaridis, T.; Mallik, B.; Chen, Y. Implicit solvent simulations of DPC micelle formation. *J. Phys. Chem. B* **2005***, 109*, 15098–15106.

Lee, Y. S. *Self-assembly and nanotechnology: a force balance approach*; John Wiley & Sons: Hoboken, New Jersey, 2008.

Lee, C. Y.; McCammon, J. A.; Rossky, P. J. The structure of liquid water at an extended hydrophobic surface. *J. Chem. Phys.* **1984***, 80*, 4448–4455.

Leung, K.; Luzar, A.; Bratko, D. Dynamics of capillary drying in water. *Phys. Rev. Lett.* **2003**, *90*, 065502/1–065502/4.

Lisiecki, I.; Billoudet, F.; Pileni, M. Control of the shape and the size of copper metallic particles. *J. Phys. Chem. B* **1996**, *100*, 4160–4166.

Maillet, J. B.; Lachet, V.; Coveney, P. V. Large scale molecular dynamics simulation of self-assembly processes in short and long chain cationic surfactants. *Phys. Chem. Chem. Phys.* **1999**, *1*, 5277–5290.

Manne, S.; Cleveland, J. P.; Gaub, H. E.; Stucky, G. D.; Hansma, P. K. Direct visualization of surfactant hemimicelles by force microscopy of the electrical double layer. *Langmuir* **1994**, *10*, 4409–4413.

Manne, S.; Gaub, H. E. Molecular organization of surfactants at solid-liquid interfaces. *Science* **1995**, *270*, 1480–1482.

McQuarrie, D. A. *Statistical Mechanics*; Harper and Row: New York, 1975.

Mileva, E. Static Structure of Polydisperse Micellar Solutions. *J. Colloid Interface Sci.* **2000**, *232*, 211–218.

Mittal, K. L. *Micellization, solubilization, and microemulsions*, Vol. 1; Plenum Press: New York, 1977.

Morisada, S.; Shinto, H.; Higashitani, K. Revised implicit solvent model for the simulation of surfactants in aqueous solutions. *J. Phys. Chem. B* **2005**, *109*, 11762–11769.

Morisada, S.; Shinto, H. Implicit Solvent Model Simulations of Surfactant Self-Assembly in Aqueous Solutions. *J. Phys. Chem. B* **2010**, *114*, 6337–6343.

Morishita, T. Fluctuation formulas in molecular-dynamics simulations with the weak coupling heat bath. *J. Chem. Phys.* **2000**, *113*, 2976–2982.

Mueter, D.; Shin, T.; Deme, B.; Fratzl, P.; Paris, O.; Findenegg, G. H. Surfactant Self-Assembly in Cylindrical Silica Nanopores. *J. Phys. Chem. Lett.* **2010**, *1*, 1442–1446.

Nagarajan, R.; Ruckensteine, E. Theory of Surfactant Self-Assembly - a Predictive Molecular Thermodynamic Approach. *Langmuir* **1991**, *7*, 2934–2969.

NRL. The Ideal beta Cristobalite (C9) Structure http://cst-www.nrl.navy.mil/lattice/struk/c9.html (accessed 8/15/2010, 2010).

Pasquali, M. Gelation: Grow with the flow. *Nat. Mater.* **2010**, *9*, 381–382.

Patrick, H.; Warr, G.; Manne, S.; Aksay, I. Self-assembly structures of nonionic surfactants at graphite/solution interfaces. *Langmuir* **1997***, 13*, 4349–4356.

Picquart, M.; Lacrampe, G. Raman spectra of aqueous sodium octanoate solutions: solute and solvent study. *J. Phys. Chem.* **1992***, 96*, 9114–9120.

Pileni, M. P. Nanosized Particles Made in Colloidal Assemblies. *Langmuir* **1997***, 13*, 3266–3276.

Puvvada, S.; Blankschtein, D. Molecular-Thermodynamic Approach to Predict Micellization, Phase-Behavior and Phase-Separation of Micellar Solutions .1. Application to Nonionic Surfactants. *J. Chem. Phys.* **1990***, 92*, 3710–3724.

Puvvada, S.; Blankschtein, D. Thermodynamic Description of Micellization, Phase-Behavior, and Phase-Separation of Aqueous-Solutions of Surfactant Mixtures. *J. Phys. Chem.* **1992a***, 96*, 5567–5579.

Puvvada, S.; Blankschtein, D. Theoretical and Experimental Investigations of Micellar Properties of Aqueous-Solutions Containing Binary-Mixtures of Nonionic Surfactants. *J. Phys. Chem.* **1992b***, 96*, 5579–5592.

Rassing, J.; Sams, P. J.; Wyn-Jones, E. Kinetics of micellization from ultrasonic relaxation studies. *J. Chem. Soc. , Faraday Trans. 2* **1974***, 70*, 1247–1258.

Reimer, U.; Wahab, M.; Schiller, P.; Mogel, H. Monte Carlo study of surfactant adsorption on heterogeneous solid surfaces. *Langmuir* **2005***, 21*, 1640–1646.

Rodriguez-Pulido, A.; Casado, A.; Munoz-Ubeda, M.; Junquera, E.; Aicart, E. Experimental and Theoretical Approach to the Sodium Decanoate-Dodecanoate Mixed Surfactant System in Aqueous Solution. *Langmuir* **2010***, 26*, 9378–9385.

Rosen, M. J. *Surfactants and Interfacial Phenomena*., 3rd ed.; John Wiley & Sons: New Jersey, **2004**.

Roy, S. B.; Dzombak, D. A. Chemical factors influencing colloid-facilitated transport of contaminants in porous media. *Environ. Sci. Technol.* **1997***, 31*, 656–664.

Sahimi, M. Flow phenomena in rocks: from continuum models to fractals, percolation, cellular automata, and simulated annealing. *Rev. Mod. Phys.* **1993***, 65*, 1393–1534.

Sammalkorpi, M.; Sanders, S.; Panagiotopoulos, A. Z.; Karttunen, M.; Haataja, M. Simulations of Micellization of Sodium Hexyl Sulfate. *J. Phys. Chem. B* **2011***, 115*, 1403–1410.

Sanders, S. A.; Panagiotopoulos, A. Z. Micellization behavior of coarse grained surfactant models. *J. Chem. Phys.* **2010***, 132*, 114902/1–114902/9.

Schramm, L. L.; Stasiuk, E. N.; Marangoni, D. G. Surfactants and their applications. *Annu. Rep. Prog. Chem. Sect. C: Phys. Chem.* **2003***, 99*, 3–48.

Schuler, L. D.; Daura, X.; Van Gunsteren, W. F. An improved GROMOS96 force field for aliphatic hydrocarbons in the condensed phase. *J. Comput. Chem.* **2001***, 22*, 1205–1218.

Schuttelkopf, A.; van Aalten, D. PRODRG: a tool for high-throughput crystallography of protein-ligand complexes. *Acta Crystallogr. D* **2004***, 60*, 1355–1363.

Shah, K.; Chiu, P.; Sinnott, S. B. Comparison of morphology and mechanical properties of surfactant aggregates at water-silica and water-graphite interfaces from molecular dynamics simulations. *J. Colloid Interface Sci.* **2006***, 296*, 342–349.

Shah, K.; Chiu, P.; Jain, M.; Fortes, J.; Moudgil, B.; Sinnott, S. Morphology and mechanical properties of surfactant aggregates at water-silica interfaces: Molecular dynamics simulations. *Langmuir* **2005***, 21*, 5337–5342.

Shiloach, A.; Blankschtein, D. Measurement and prediction of ionic/nonionic mixed micelle formation and growth. *Langmuir* **1998***, 14*, 7166–7182.

Shinto, H.; Morisada, S.; Miyahara, M.; Higashitani, K. Langevin dynamics simulations of cationic surfactants in aqueous solutions using potentials of mean force. *Langmuir* **2004***, 20*, 2017–2025.

Shinto, H.; Morisada, S.; Miyahara, M.; Higashitani, K. A reexamination of mean force potentials for the methane pair and the constituent ion pairs of NaCl in water. *J. Chem. Eng. Japan* **2003***, 36*, 57–65.

Soderman, O.; Johansson, I. Polyhydroxyl-based surfactants and their physico-chemical properties and applications. *Curr. Opin. Colloid Interface Sci.* **1999***, 4*, 391–401.

Sogami, I. Effective Potential between Charged Spherical-Particles in Dilute Suspension. *Phys. Lett. A* **1983***, 96*, 199–203.

Sohrabi, B.; Bazyari, A.; Hashemianzadeh, M. Effect of ethylene glycol on micellization and surface properties of Gemini surfactant solutions. *Colloids Surf. Physicochem. Eng. Aspects* **2010***, 364*, 87–93.

Sohrabi, B.; Gharibi, H.; Javadian, S.; Hashemianzadeh, M. A New Model to Study the Phase Transition from Microstructures to Nanostructures in Ionic/Ionic Surfactants Mixture. *J. Phys. Chem. B* **2007***, 111*, 10069–10078.

Somasundaran, P.; Huang, L. Adsorption/aggregation of surfactants and their mixtures at solid–liquid interfaces. *Adv. Colloid Interface Sci.* **2000***, 88*, 179–208.

Srinivasan, V.; Blankschtein, D. Effect of counterion binding on micellar solution behavior: 1. Molecular-thermodynamic theory of micellization of ionic surfactants. *Langmuir* **2003***, 19*, 9932–9945.

Stephenson, B.; Beers, K.; Blankschtein, D. Complementary use of simulations and molecular-thermodynamic theory to model micellization. *Langmuir* **2006***, 22*, 1500–1513.

Striolo, A.; Prausnitz, J. M. Adsorption of branched homopolymers on a solid surface. *J. Chem. Phys.* **2001***, 114*, 8565–8572.

Tanford, C. *The Hydrophobic Effect: Formation of Micelles and Biological Membranes*; Wiley: New York, 1980.

Trompette, J.; Zajac, J.; Keh, E.; Partyka, S. Scanning of the Cationic Surfactant Adsorption on a Hydrophilic Silica Surface at Low Surface Coverages. *Langmuir* **1994***, 10*, 812–818.

Tulpar, A.; Ducker, W. Surfactant adsorption at solid-aqueous interfaces containing fixed charges: Experiments revealing the role of surface charge density and surface charge regulation. *J. Phys. Chem. B* **2004***, 108*, 1667–1676.

Tummala, N. R.; Striolo, A. Role of counterion condensation in the self-assembly of SDS surfactants at the water-graphite interface. *J. Phys. Chem. B* **2008***, 112*, 1987–2000.

Tummala, N. R.; Grady, B. P.; Striolo, A. Lateral confinement effects on the structural properties of surfactant aggregates: SDS on graphene. *Phys. Chem. Chem. Phys.* **2010***, 12*, 13137–13143.

van der Spoel, D.; Lindahl, E.; Hess, B.; van Buuren, A. R.; Apol, E.; Meulenhoff, P. J.; Tieleman, D. P.; Sijbers, A. L. T. M.; Feenstra, K. A.; van Drunen, R.; Berendsen, H. J. C. *GROMACS User Manual Version 3.3*; www.gromacs.org, 2005.

Vasudevan, M.; Buse, E.; Lu, D.; Krishna, H.; Kalyanaraman, R.; Shen, A. Q.; Khomami, B.; Sureshkumar, R. Irreversible nanogel formation in surfactant solutions by microporous flow. *Nat. Mater.* **2010***, 9*, 436–441.

Velegol, S. B.; Fleming, B. D.; Biggs, S.; Wanless, E. J.; Tilton, R. D. Counterion Effects on Hexadecyltrimethylammonium Surfactant Adsorption and Self-Assembly on Silica. *Langmuir* **2000***, 16*, 2548–2556.

Verwey, E. J. W.; Ovrbeek, J. T. G. *Theory of Stability of Lyophobic colloids;*Elsevier: Amsterdam, 1948.

Wang, Y.; Wang, Y.; Chen, K.; Li, B. Non-equilibrium molecular dynamics simulation of electrokinetic effects on heterogeneous ionic transport in nano-channel. *Chem. Eng. Sci.* **2011***, 66*, 2807–2816.

West, C. C.; Harwell, J. H. Surfactants and subsurface remediation. *Environ. Sci. Technol.* **1992***, 26*, 2324–2330.

Xu, Z.; Yang, X.; Yang, Z. On the mechanism of surfactant adsorption on solid surfaces: Free-energy investigations. *J. Phys. Chem. B* **2008***, 112*, 13802–13811.

Yang, S. C. Effects of surface roughness and interface wettability on nanoscale flow in a nanochannel. *Microfluid. Nanofluid.* **2006***, 2*, 501–511.

Yu, K.; Steele, A.; Zhu, J.; Fu, Q.; Tsang, S. Synthesis of well-dispersed nanoparticles within porous solid structures using surface-tethered surfactants in supercritical CO_2. *J. Mater. Chem.* **2003***, 13*, 130–134.

Yuet, P. K. A simulation study of electrostatic effects on mixed ionic micelles confined between two parallel charged plates. *Langmuir* **2004***, 20*, 7960–7971.

Yuet, P.; Blankschtein, D. Molecular-thermodynamic modeling of mixed cationic/anionic vesicles. *Langmuir* **1996***, 12*, 3802–3818.

Zemb, T.; Drifford, M.; Hayoun, M.; Jehanno, A. Light scattering study of solutions of sodium octanoate micelles. *J. Phys. Chem.* **1983***, 87*, 4524–4528.

Zettlemoyer, A. Hydrophobic Surfaces. *J. Colloid Interface Sci.* **1968***, 28*, 343–369.

Zhang, X.; Chen, G.; Wang, W. Confinement induced critical micelle concentration shift. *J. Chem. Phys.* **2007***, 127*, 034506/1–034506/7.

Zhu, W.; Singer, S. J.; Zheng, Z.; Conlisk, A. T. Electro-osmotic flow of a model electrolyte. *Phys. Rev. E.* **2005***, 71*, 041501/1–041501/12.